

RSC Advances



This is an *Accepted Manuscript*, which has been through the Royal Society of Chemistry peer review process and has been accepted for publication.

Accepted Manuscripts are published online shortly after acceptance, before technical editing, formatting and proof reading. Using this free service, authors can make their results available to the community, in citable form, before we publish the edited article. This *Accepted Manuscript* will be replaced by the edited, formatted and paginated article as soon as this is available.

You can find more information about *Accepted Manuscripts* in the [Information for Authors](#).

Please note that technical editing may introduce minor changes to the text and/or graphics, which may alter content. The journal's standard [Terms & Conditions](#) and the [Ethical guidelines](#) still apply. In no event shall the Royal Society of Chemistry be held responsible for any errors or omissions in this *Accepted Manuscript* or any consequences arising from the use of any information it contains.

**Recent developments in heterogeneous photocatalytic water
treatment using visible-light-responsive photocatalysts: A review**

Shuying Dong^a, Jinglan Feng^a, Maohong Fan^{c,d}, Yunqing Pi^a, Limin Hu^a, Xiao Han^a,
Menglin Liu^a, Jingyu Sun^{b1}, Jianhui Sun^{a2}

^a *School of Environment, Henan Normal University, Key Laboratory for Yellow River
and Huai River Water Environmental and Pollution Control, Ministry of Education,
Henan Key Laboratory for Environmental Pollution Control, Xinxiang, Henan
453007, P. R. China*

^b *Center for Nanochemistry (CNC), College of Chemistry and Molecular Engineering,
Peking University, Beijing 100871, P. R. China*

^c *Department of Chemical and Petroleum Engineering, University of Wyoming, 1000 E
University Avenue, Laramie, WY 82071, USA*

^d *School of Civil and Environmental Engineering, Georgia Institute of Technology,
Atlanta, Georgia 30332, USA*

¹ Corresponding author. E-mail: sunjy-cnc@pku.edu.cn (J.Y. Sun). Tel.: +86-10-62757157

² Corresponding author. E-mail: sunjh@htu.cn (J.H. Sun). Tel.: +86-373-3325971

Abstract

Visible-light-responsive photocatalytic technology holds great potential in water treatment to enhance the purification efficiency as well as augment water supply throughout the safe usage of unconventional water sources. This review summarizes the recent progress in the design and fabrication of visible-light-responsive photocatalysts *via* various synthetic strategies including modification of traditional photocatalysts by doping, dye sensitization, forming heterostructure, coupled with π -conjugated architecture, as well as in the great efforts made within the exploration of novel visible-light-responsive photocatalysts. The background on fundamentals of heterogeneous photocatalysis, pathways of visible-light-responsive photocatalysis, and unique features of visible-light-responsive photocatalysts are presented. The photocatalytic properties of the resulting visible-light-responsive photocatalysts are also covered in relation to the water treatment regarding the photocatalytic degradation of organic compounds, inorganic pollutants, as well as photocatalytic disinfection. Finally, this review concludes with a summary and perspectives on the current challenges faced and new directions in this emerging area of research.

Keywords: visible-light-responsive; photocatalytic; water treatment; regulatory mechanism; physicochemical properties;

1. Introduction

With the rapid development of industrialization, urbanization as well as population, the urgent demand and acute shortage of clean water sources have attracted great attention all over the world. This situation is expected to continue to deteriorate with respect to the growing contamination, owing to the overwhelming discharge of contaminants and pollutants into the natural water cycle. As far as the environment is concerned, the reuse and recycle of wastewater effluents is necessary for augmenting the limited fresh water supply and offsetting more possible water resources in the long run.¹ During the past decades, a variety of practical strategies have been implemented to develop viable wastewater treatment technologies.²⁻⁶ For instance, conventionally biological treatments were designed to effectively eliminate assorted types of contaminants from wastewater in the short term, however, these techniques could normally lead to the production of secondary pollution,⁷ some of which even associated with the presence of health-threatened bacteria and soluble refractory organic compounds that are hard to be removed.⁸ In this regard, developing non-destructive, green and sustainable methodologies for water treatment is hence of great significance.

To date, photocatalysis has been considered as one of the most appealing options for wastewater treatment due to its great potential and high efficiency by using sunlight to remove organic pollutants and harmful bacteria with the aid of a solid photocatalyst.^{9,10} It is well known that the photocatalytic efficiency is not only influenced by the nature of the employed photocatalysts, but also affected by the

irradiated light source. Generally, the catalyst can be photo-activated by a photon with energy equal to or higher than its band gap energy (E_g). Stronger irradiation intensity would normally induce more efficient photolysis reactions.¹¹ As a safe and renewable energy source, natural sunlight is the ideal to supply energy for these activation processes. Moreover, solar energy possesses special advantages such as cleanness and abundance. The sun delivers about 4 orders of magnitude larger energy to the earth's surface per year than the energy annually used by humans all over the world.^{12, 13} To better utilize the solar energy to tackle the water contamination issues, it is strongly desirable to explore catalysts with visible-light-driven photocatalytic performance.

TiO₂ is the most widely studied photocatalyst due to its cost-effectiveness, nontoxicity, unique photocatalytic efficiency as well as high stability. The basic mechanism of photocatalytic degradation of pollutants using TiO₂ deals with the absorption of the near-UV ranged light by TiO₂, the input of light energy inducing charge separation to form electron (e^-)-hole (h^+) pairs, and the participation of e^- and h^+ in the oxidation-reduction reactions with suitable substrates.¹⁴ However, the drawbacks of pure TiO₂ in photocatalysis are concerned with the relatively large band-gap and the related fact that it can only absorb a small portion of UV radiation.¹⁵ To facilitate the usage of energy from natural sunlight, certain routes have been attempted to modify TiO₂ accordingly, which includes non-/transition-metal ion doping,^{16,17} sensitization,¹⁸ ion implantation,¹⁹ narrower band-gap semiconductor coupling,²⁰ and π -conjugated structure compositing²¹ *etc.* For example, Rey *et al.*¹⁶ synthesized TiO₂-WO₃ photocatalysts, which exhibited higher catalytic activity than

that of pure TiO₂ for the removal of a mixture of emerging contaminants through photocatalytic ozonation under visible light radiation. A study conducted by our group demonstrated that nitrogen-doped TiO₂ showed superior photocatalytic performance than that of the commercial Dugussa P25 TiO₂ for the degradation of a specific azo dye (Orange G) under visible light irradiation, which was attributed to the fact that nitrogen doping gave rise to the appearance of new absorption band in the visible region.¹⁷

There has been a growing interest lately in the development of directly visible-light-responsive photocatalysts for water treatments, partially due to the reason of the complex and costly steps in the modification of UV-illuminated ones.²² To this end, a plethora of photocatalysts have been created, e.g. SnS₂,²³ CuO/BiVO₄,²⁴ ZnS,²⁵ g-C₃N₄/BiPO₄,²⁶ AgBr/Ag₃PO₄/MWCNTs,²⁷ Ag₃PO₄,²⁸ BiOX (X = Cl, Br, I),²⁹ Bi₂MO₆ (M = W, Mo),^{30,31} and MWO₄ (M²⁺ = Co, Cu, Pb, Cd, Mn and Zn),³² ZnSnO₃,³³ MVO₄ (M = Bi, Sm),^{34,35} nanostructured iron (III) oxides,³⁶ oxynitride,³⁷ where considerable advances with regard to the photocatalytic performances have been steadily achieved, opening up the possibility in the practical usage of natural solar energy for the wastewater degradation as well as the environmental protection. For example, Mondal *et al.*²³ have demonstrated that the dosage of variable concentrations of thioacetamide enabled the congregation of SnS₂ nanoflakes to nanoflowers and nanoyarns, which were proven to be promising for promoting photoreduction of toxic Cr(VI) wastewater under visible light irradiation. Moreover, the performance of SnS₂ nanoflower was found to be superior to that of nanoyarn,

owing to the increased surface area and higher pore volume. Sheng *et al.*³⁰ have probed the photocatalytic activities of Bi₂WO₆ under visible light conditions using phenol degradation as a model reaction, where the observations obtained by employing spin-trapping electron paramagnetic resonance spectroscopy indicated that the irradiated Bi₂WO₆ was responsible not only for the production of ·OH radicals (*via* water oxidation), but also for the generation of H₂O₂ (*via* two-electron reduction of O₂).

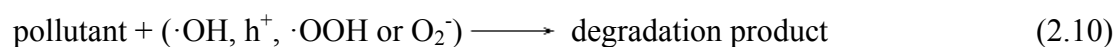
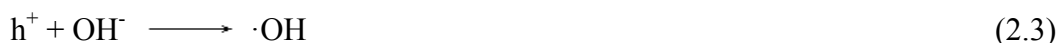
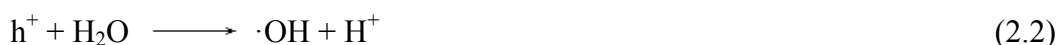
From practical application points of view, solid substrate supported photocatalysts have in particular been recognized as an important class of industrial catalysts that are closely related with versatile key technologies in the water treatment. The supported catalysts were investigated to possess several advantages such as improved resistance to agglomeration, good accessibility of substrate molecules, site isolation, practical usage in continuous-flow systems, and mechanical robustness, etc.^{19,22,38-41} Moreover, such materials enabled the direct integration of technological devices to improve the photocatalysts' activity.³⁹ For example, Carraro *et al.*⁴⁰ prepared polymorphs iron (III) oxide nanosystems [α -Fe₂O₃ (hematite) and β -Fe₂O₃ (bixbyite)] *via* chemical vapor deposition approach, which were well characterized and tested in the photo-degradation of methylene blue (MB) in the liquid phase under simulated solar light irradiation. The obtained results showed a significant dependence of the purity and morphology on the synthetic conditions, where the surface area of the sample appeared to have a crucial influence on the photocatalytic performances. Aziz *et al.*⁴¹ fabricated magnetically separable TiO₂ nanocomposite

with SiO₂ coating (supported on a permanent magnet NiFe₂O₄), the prepared TiO₂ material was featured by a lower band gap energy (2.26 eV) and higher visible light absorption than that of pure TiO₂ (2.76 eV). Accordingly, the nanocomposite exhibited an improved sunlight activity for the photodegradation of 2,4-dichlorophenol, as well as a good stability against the loss of magnetic property for reuse.

This field of research has stimulated great efforts on the preparation, modification, and application of visible-light-responsive photocatalysts with many important findings reported during the past years. Many insightful review articles have dealt with the target synthesis, theoretical investigation, photocatalysis design, and possible applications of photocatalysts, esp. centering on the specific modification of certain types of photocatalysts. In contrast, few reviews were concerned with the discussion of photocatalysis in a broader context of visible-light-responsive photocatalyst types, *i.e.* the routes to affording the visible-light responses, the effects of corresponding properties, and the related application within the water treatments. Based on the aforementioned facts, this review summarizes the latest developments of visible-light-responsive photocatalysis, with a focus on the broad coverage of employed catalyst systems. It starts with a brief introduction of fundamentals and speculated mechanisms of visible-light-responsive photocatalysis, followed by the discussion of recent achievements in the design, modification, and applications of visible-light-responsive photocatalyst systems. Outlooks and perspectives in the future directions are also included at the end.

2. Fundamentals and proposed pathways of visible-light-responsive photocatalysis

In general, the system of heterogeneous photocatalysis using semiconductor material consists of a light harvesting antenna and several active species to facilitate the pollutant degradation. The series of chain oxidative-reductive reactions that occur at the photon activated surface were broadly proposed as follows:



When the semiconductor is irradiated by an input light possessing ultra-band-gap energy ($h\nu > E_g$), a valence band (VB) electron (e^-) is excited to the conduction band (CB), leaving a photogenerated hole (h^+) at the VB. Accordingly, the produced e^-/h^+ pairs are able to migrate to the surface of the semiconductor and participate in the redox reactions. The photocatalytic reaction usually involves three main active species: hydroxyl radical ($\cdot\text{OH}$), h^+ , and superoxide radical ($\cdot\text{O}_2^-$), where $\cdot\text{OH}$ is the primary

oxidant in the photocatalytic degradation of pollutant in the aqueous solution. The generation of $\cdot\text{OH}$ radicals is normally concerned with two routes, (i) H_2O and OH^- in the water environment can be readily oxidized by photogenerated h^+ to form $\cdot\text{OH}$ radicals; (ii) O_2 presented in the aqueous solution can be reduced by photogenerated e^- to form $\cdot\text{O}_2^-$ radicals, followed by reacting with h^+ (forming $\cdot\text{OOH}$ radicals) and further decomposition to produce $\cdot\text{OH}$ radicals. Moreover, the photogenerated h^+ has been widely considered as an oxidant to directly degrade organic contaminates, the capacity of which relies on the catalyst types and oxidation conditions.⁴² It is noted that the photo-induced e^- can easily recombine with h^+ after their generation in the absence of electron or hole scavengers. In this regard, the presence of specific scavengers is vital for suppressing the charge recombination rates and enhancing the efficiency of photocatalysis.

To design a photocatalyst capable of utilizing safe and sustainable solar energy effectively, several critical requirements need to be satisfied. First of all, the semiconductor material should have a smaller band gap to allow to absorbing solar energy across a broad range of spectrum. Simultaneously, the semiconductor should have a relatively positive enough valence band for the ample production of h^+ and $\cdot\text{OH}$ radicals.⁴³ Secondly, the catalyst should possess a particular platform/system for the efficient charge separation and transportation.^{44,45} Moreover, the semiconductor materials should have good photoelectrochemical stability in the electrochemical reactions.⁴⁶

Generally, along with electronic band structures, other features such as the

material choice, morphological architecture, crystallinity, and surface properties should also be taken into consideration when building-up an efficient and stable visible-light-responsive photocatalytic system.^{47,48} The choice of the semiconductor materials is particularly important since it determines the level of the visible-light-response and hence the overall efficiency. The morphological architecture with short distance between photocarrier generating junction and redox reaction center can effectively improve the carrier separation and transportation.⁴⁹ Moreover, a high degree of crystallinity with crystal defects would minimize the interface recombination, thereby enhancing the efficiencies of photogenerated electrons and holes for desired reactions.⁵⁰ The surface area of photocatalysts, which depends upon the porosity and geometrical shape of the materials, also exerts a crucial effect on the photocatalytic activity, owing to the fact that the adsorption of pollutants is a critical step.⁵¹

3. Overview of visible-light-responsive photocatalysts

3.1. Modification routes towards augmenting visible-light-response of photocatalysts

Compared to other photocatalysts for wastewater treatment, TiO₂ and ZnO have received considerable attention due to their advanced photocatalytic performance under UV light irradiation.^{52,53} The drawback of those semiconductors, however, lies in the fact that they are inactive under visible light irradiation due to their large band gap, which impedes their usage as solar energy harvesting photocatalysts. To overcome such vital deficiency, certain modifications toward the semiconductors system have been attempted to enable their visible-light-responses with good efficiency.

3.1.1. Doping

Doping plays an indispensable role in modifying the properties of functional photocatalyst materials, which, in particular non-metal doping, has been intensively investigated, since nitrogen-doped TiO₂ was initially reported by Asahi and colleagues.⁵⁴ The effect of doping on the properties of photocatalyst is governed by several factors, such as the type and concentration of the dopant, fabrication method and physicochemical properties of the intrinsic catalyst. Previous studies have indicated that non-metal doping possesses great potential in realizing visible-light-responsive photocatalytic activity, in this regard, a plethora of non-metals have been explored as dopants in modifying the electronic structure of UV-illuminated semiconductors.⁵⁵ In particular, non-metal doping at the atomic level could preserve the inherent surface properties of the photocatalyst, since the dopants exist as the forms of isolated atoms rather than clusters within the surface.⁵⁶ Furthermore, the special distribution of dopant states is generally located closely above the VB maximum, making the photo-generated holes on these states oxidative enough for subsequent photo-reactions.⁵⁷

Nitrogen doping has been intensively studied amongst all the non-metal dopants. Wang *et al.*⁵⁸ prepared N-doped TiO₂ by heat treatment of commercial P25-TiO₂ in a NH₃ gas flow and the product was characterized by a series of techniques to investigate the origin of visible light response of N-doped TiO₂. The results indicated that N-doped TiO₂ possessed triplet g value electron spin resonance signals ($g = 1.987, 2.004$ and 2.024) and visible light absorption in a wavelength range of 400-520 nm,

which were attributed to the formation of single-electron-trapped oxygen vacancy (denoted as SETOV) in a certain chemical environment. The visible light photocatalytic activity of N-doped TiO₂ was co-determined by the formation of SETOV in TiO₂ matrix and existence of doped-N on the surface. Similarly, one of our previous studies also reported that N-doped TiO₂ showed higher photocatalytic activity than that of the commercial Dugussa P25 TiO₂ under visible light irradiation, which could be due to the presence of TiO₂ anatase structure and the new absorption band in the visible region caused by the nitrogen doping¹⁷.

Carbon doping has been explored with the consideration of its low cost and the potential of band-gap narrowing, achieving significant improvements in visible light absorption capability.⁵⁹⁻⁶² Chen *et al.*⁶⁰ synthesized pure anatase C-doped TiO₂ by low-pressure flat-flame metal organic chemical vapor condensation method by eliminating the nitrogen doping possibility. They demonstrated that visible-light absorption was attributed to the carbon doping, and the carbon did not incorporate into the TiO₂ crystal but instead locate on the surface. They also claimed that the C-C bond was responsible for the light absorption. Dai and colleagues⁶¹ prepared porous C-doped Bi₂O₃ with high visible-light-response photocatalytic activity *via* simple calcination of bismuth nitrate pentahydrate in a glycol solution. It was shown that the carbon was incorporated into the lattice of Bi₂O₃, the absorption edge C-doped Bi₂O₃ had an obvious red shift with augmented absorption intensity in the region of 450-530 nm, which was responsible for the enhanced photocatalytic activity than that of the pure one. Samadi and coauthors⁶² utilized electrospinning technique to fabricate

multi-walled carbon nanotube (MWCNT) doped ZnO nanofibers with visible-light-response photocatalytic activity. Their study revealed that Zn-O-C bonds were formed and the energy band gap of the composite was 2.94 eV, which was lower than that of the pure ZnO nanofiber (3.11 eV). Accordingly, a 7-fold enhancement in the photocatalytic activity was observed because of the delayed electron-hole recombination exerted by the synergistic effect between MWCNT and ZnO. However, compared to the N-doped photocatalysts, C-doped ones have been deemed to be more difficult to synthesize and hence have not been widely employed to date.⁶³

Modifications of photocatalyst with noble and other metals such as Pt, Au, Ag, Cu, V, Ni and Sn have also enabled the extension of the spectral response of photocatalysts well into the visible region.⁶⁴ However, few studies claimed that several metallic species (esp. transition metals) may act as recombination sites for the photo induced charge carriers, therefore lowering the quantum efficiency.⁶⁵ For instance, Li *et al.*⁶⁵ fabricated hierarchical V-doped rutile TiO₂ nanofibers by a flame burning method, which showed higher doping level of V into TiO₂ crystal lattices than that prepared by calcination treatments. The photocatalytic activity of the synthesized V-doped rutile TiO₂ nanofibrous have not yet been obviously enhanced due to the V doping, which could be attributed to the fact that the V dopants served as electron-hole recombination centers. Vijayan *et al.*⁶⁶ prepared visible light activated Pt-TiO₂ nanotubes by a hydrothermal technique, where Pt doping affected the morphology of the TiO₂ nanotubes. Their study revealed that Pt nanoparticles were uniformly distributed on the nanotube surface and the doping by Pt enhanced the

visible light photoactivity of TiO₂ nanotubes for the photo-oxidation of acetaldehyde. Electron paramagnetic resonance spectra revealed that coordinated sites and oxygen deficiency were created on the surface of the TiO₂ nanotube after calcination in a hydrogen atmosphere, which further interacted with the Pt centers to alter the electronic, optical and chemical behavior of the TiO₂ nanotube. One of our recent studies has reported the synthesis of Sn-doped ZnO photocatalysts with augmented sunlight photocatalytic activity throughout a microwave-assisted route. The microstructure, morphology and optical properties of ZnO were greatly changed by the Sn doping, contributing to the enhancement of enhanced sunlight photocatalytic activity (a 13% higher decolorization rate and 29-52% greater mineralization efficiency than that of pure ZnO for the degradation of MB solution).⁶⁷

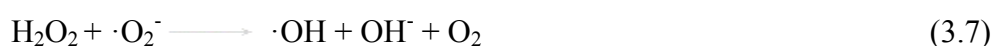
Co-doping with two or more suitable heteroatoms (nonmetal-nonmetal, metal-nonmetal, and metal-metal) can lead to substantially synergistic effects with respect to changing the band structures (including CB and VB levels) of the systems to obtain desired photocatalytic redox ability and selectivity, enhancing visible-light harvesting and charge mobility, or modifying the morphological characteristics. Moafi and colleagues⁶⁸ prepared La-Zr-doped ZnO nanocomposites using a modified sol-gel method. Their characterization indicated that La-Zr-doped ZnO exhibited a smaller particle size than that of pure ZnO with a red-shift feature in the absorption band. Interestingly, the co-doping of the La and Zr gave rise to the band-gap narrowing as well as the photo-activity enhancement. Wu *et al.*⁶⁹ synthesized C-N co-doped TiO₂ hierarchical spheres *via* a direct chelating process with the aid of several types of

amine agents, where it was found that the optimal C and N doping concentrations were produced by using trimethylamine, which effectively reduced the band-gap of TiO₂ to 2.85 eV without affecting its crystallization. Moreover, it exhibited eightfold photocatalytic activity higher than that of commercial Degussa P25 powders for the decomposition of Rhodamine B (RhB). Sun *et al.*⁷⁰ prepared N-TiO₂, Pt-TiO₂, N-Fe-TiO₂, N-Ni-TiO₂, N-Ag-TiO₂ and N-Pt-TiO₂ photocatalysts by acid-catalyzed sol-gel processes, further evaluated the corresponding photocatalytic activities *via* the photodegradation of phenol solutions under simulated sunlight irradiation. It is worth-noting that certain types of transition metals (Fe and Ni in this case) exerted a negative effect on N-metal co-doped TiO₂ photocatalysis, whilst noble metals (Ag and Pt) showed augmentation in photocatalysis. In particular, N-Pt-TiO₂ exhibited a six times higher photocatalytic efficiency than that of Degussa P25 under simulated sunlight irradiation. The synergistic effect of N-Pt co-doping was ascribed to the multivalent states of Pt.

3.1.2. Dye sensitization

A simple and interesting strategy for achieving effective visible light harvesting is the photosensitization of wide-band-gap semiconductors by appropriate sensitizer molecules. Dye photosensitization has been reported to be one of the most promising ways to extend the photoresponse into the visible region and to possess certain advantages over the direct photocatalysis.⁷¹⁻⁷⁵ The visible light induced photocatalytic mechanism of the dye sensitized photocatalyst was proposed as follows⁷¹:





The dye can absorb the visible light to reach an excited state, which, in general, has lower redox potential than that of the corresponding ground state. When the redox potential is lower than the CB of the semiconductor, the cationic radicals and conduction band electron can be formed easily if an electron injected into the conduction band from the excited state.^{71,72} Li *et al.*⁷² showed that photo-response of the squarylium dye (ISQ) sensitized TiO₂ nanoparticles were remarkably extended to visible-light region and the photocatalytic activity under visible light irradiation were significantly enhanced. In such system, the ISQ dye on the sensitized surface of TiO₂ could be easily excited from the ground state (D) to the excited state (D*) with the aid of the visible light. This excited state dye species can be converted to a semi-oxidized radical cation ($\cdot\text{D}^+$) by the injection of an electron into the CB of TiO₂, owing to the reason that the lowest unoccupied molecular orbital (LUMO) level of ISQ dye matched well with the CB of TiO₂, benefiting the charge transfer. Radicals such as $\cdot\text{O}_2^-$, $\cdot\text{OH}$ and $\cdot\text{OOH}$ were then produced *via* a series of protonation and reduction steps. Finally, the $\cdot\text{OH}$ radicals reacted with MB molecules to produce the degradation

product.

Furthermore, the transportation of molecules adsorbed on the surfaces is reduced at a dimensional level, which is beneficial to reaction kinetics and results in the extension of the excitation energy range of a semiconductor into the visible region. It may possess the capability to drive other reactions, and hence the sensitivity of the photocatalytic process for removal of colored pollutants will be increased in the presence of low concentrations of colored pollutants.⁷³ This approach is useful for treating textile wastewater, and one of the consequences is the direct oxidation of the dye. Shang *et al.*⁷⁴ demonstrated that the enhanced photocatalytic activity of dye sensitized TiO₂ was attributed to the wider absorption spectrum range and the electron transferred from the excited state of the dye molecule directly to the CB of TiO₂, which result in a greater number of electrons in the CB of TiO₂ and consequent production of more active oxygen species. Li *et al.*⁷⁵ found that sensitized ZnO microrods with porphyrin hetero-aggregate result in an enhanced visible light photocatalytic activity compared to those of the porphyrin monomers modified ZnO and pure ZnO, which might be attributed to the redox potential of the porphyrin hetero-aggregate matched well with the energy level of ZnO and the consequent promotion of the electron injection from the excited state of porphyrin into the CB of ZnO, correspondingly suppressing the electron-hole recombination rates. Yang *et al.*⁷⁶ probed the usage of Alizarin Red S dye-sensitized nanoscale ZnO for the photocatalytic removal of Cr⁶⁺ from the aqueous solution under visible light irradiation. The apparent band gap energy of the dye-sensitized nanoscale ZnO (2.79

eV) was narrower compared with that of nanoscale ZnO without dye sensitization (3.37 eV). The dye molecule, acting as an organic semiconductor, might exert an effect on the charge transition into the CB of ZnO in the excited state.

3.1.3. Heterostructure

Heterostructured semiconductor is another class of photocatalysts that utilizes visible light for the photocatalytic water treatment. When a wide band-gap semiconductor is coupled with a narrow band-gap semiconductor with a more negative CB level, enhanced electron-hole separation will be achieved since the CB electrons can be injected from the narrow band-gap semiconductor to the wide band-gap semiconductor. Furthermore, the visible light response is originated from the visible-light photocatalytic activity of the narrow band-gap semiconductor as well as the synergistic effect in the heterostructure. The process is similar to dye sensitization except for the following two differences. One is that electrons are injected from one semiconductor to the other semiconductor, rather than the scenario from excited dye to semiconductor. The other is that the visible light harvesting antenna is from one semiconductor rather than from a dye. In this field, great efforts have been made in the synthesis of different coupled semiconductors such as $\text{TiO}_2/\text{Bi}_2\text{WO}_6$,⁷⁷ ZnO/CdSe ,⁷⁸ $\text{Ag}/\text{Ag}_3\text{PO}_4/\text{TiO}_2$,⁷⁹ CuS/ZnO ,⁸⁰ CdS/TiO_2 ,⁸¹ and $\text{Bi}_2\text{O}_2\text{CO}_3/\text{Bi}_2\text{MoO}_6$.³¹ Compared to single-phase photocatalysts, such coupled systems usually possess enhanced visible light photocatalytic activity due to the fact that heterostructured combination extends the light-response range by coupling suitable electronic structures in materials and promotes the separation of photoexcited

electron-hole pairs through various charge-transfer pathways. The heterostructure can compensate the disadvantages of the individual components by inducing a synergistic effect such as the improvement of photostability as well as keeping redox reactions at two different reaction sites. A three-dimensional $\text{TiO}_2/\text{Bi}_2\text{WO}_6$ hierarchical heterostructure was prepared for the photocatalytic decomposition of RhB in water under visible light irradiation. The improved photocatalytic performance could be ascribed to an improved light harvesting ability and an efficient separation of photon-generated carriers.⁷⁷ Meanwhile, Wu *et al.*⁷⁸ confirmed the ZnO/CdSe heterostructure exhibited improved visible-light-responsive photocatalytic efficiency compared to that of the pure ZnO , owing to the fact that the incorporation of CdSe could extend the absorption spectrum to visible light region and suppress the recombination of photogenerated electron-hole pairs. Another example goes to the study performed by Lee *et al.*⁸⁰, which revealed that CuS/ZnO nanowire heterostructure exhibited superior photocatalytic activity and cycle performance under visible light compared with that of the bare ZnO nanowire. The advanced photocatalytic activity was due to the interfacial charge transfer from the VB of the ZnO to that of the CuS , reducing CuS to Cu_2S .

In addition to the extension of light-response range and promotion of the separation of photon-generated carriers induced by the heterostructured nature, the photocatalytic performance of such coupling system is crucially related to the size, shape, and surface area of the heterostructure. Wei *et al.*⁸¹ dispersed CdS nanoparticles within the entire surface of the TiO_2 nanofibers, forming the CdS/TiO_2

hierarchical heterostructure. The enhanced photocatalytic activities of CdS/TiO₂ heterostructure might arise from the increased surface area, extended light absorption region and the favorable electrons-transfer properties. Recently, Xu *et al.*³¹ teamed up the wide band-gap Bi₂O₂CO₃ with Bi₂MoO₆ to form hierarchical Bi₂O₂CO₃/Bi₂MoO₆ heterostructured photocatalysts with superior visible light photocatalytic activity towards degradation of RhB. The Bi₂O₂CO₃/Bi₂MoO₆ heterostructure also displayed visible-light photocatalytic activity for the destruction of *E. coli* with excellent stability and recycle performance. In this regard, the photocatalytic degradation efficiency was related to the Bi/Mo molar ratio, where the highest degradation efficiency was observed with the Bi/Mo molar ratio of 2.88/1, which was approx. 55% and 97% higher than that of the pure Bi₂O₂CO₃ microspheres and Bi₂MoO₆ nanoplatelets, respectively. Moreover, Zhou *et al.*⁸² claimed that energy-band matching was responsible for the enhanced photocatalytic activity within the heterostructured systems by carrying out a comparison study between the PdO/TiO₂ and Pd/TiO₂ heterostructured nanobelts.

3.1.4. Coupled with π -conjugated structure

In recent years, photocatalyst hybridized with a π -conjugated structure material has been proved to be an effective route for enhancing visible-light-responsive photocatalytic activity. Conventional photocatalysts such as ZnO and TiO₂ unexceptionally presented superior visible light photocatalytic performances than those of the pristine after the proper hybridization with graphene,⁸³⁻⁸⁵ C₆₀,^{86,87} C₃N₄,⁸⁸ polyaniline (PANI),^{89,90} and polypyrrole (PPy)⁹¹. These π -conjugated structure

materials have shown great promise for modifying wide band-gap inorganic semiconductors in the fabrication of visible-light-responsive photocatalyst, mainly due to the presence of their π -conjugated electron systems, high mobility of charge carriers, high absorption coefficients in the visible part of the spectrum and good environmental stability. Moreover, many conjugated structure materials have also been identified as efficient photo-generated e^- transporters upon visible-light excitation. In photocatalysis, graphene (along with graphene-oxide and reduced graphene-oxide (RGO)) has been proven to be an ideal support for constructing photocatalytic composites. When graphene was introduced to hybridize with TiO_2 , it could simultaneously improve the light absorption, narrow down the band-gap, and suppress the recombination of photo-generated electron-hole pairs.⁸³ Meanwhile, Thomas *et al.*⁸⁴ decorated carboxyl functionalized few-layer graphene with TiO_2 , the obtained composites showed a remarkable improvement in visible-light-driven photocatalysis. The enhanced visible light photocatalytic activity was attributed not only to the improved electron hole mobility, but also to the enhanced surface adsorption ability for molecules through π - π interactions. Min *et al.*⁹² demonstrated that the usage of different routes to chemically anchoring TiO_2 nanoparticles onto graphene by chemical interactions, such as chemisorption, electronegativity and coordination, would lead to great enhancement of their photocatalytic activity under visible light due to the full and intimate contact through chemical bonds Ti-C and Ti-O-C, whilst there was no such enhancement under UV-light. Gayathri *et al.*⁹³ showed that the formation of ZnO/graphene composites promoted the absorption in

the visible region and enhanced visible light photocatalytic activity compared with the pristine ZnO. Very recently, our group⁹⁴ have performed the decoration of ZnO nanoclusters with the prepared RGO to form novel ZnO/RGO nanocomposites, where we found that the photocatalytic activity in the visible-light-driven degradation of metronidazole with the ZnO nanoclusters could be enhanced by coupling with RGO, attaining an approx. 32.4% increase compared with that of pure ZnO (Figure 1).

(Figure 1)

C₆₀ possessing its unique configuration and properties has been widely studied. C₆₀ has a closed-shell configuration consisting of 30 bonding molecular orbital with 60 π -electrons, which could efficiently cause a rapid photogenerated charge separation and a relatively slow charge recombination.⁹⁵ Fu *et al.*⁸⁶ found that C₆₀-hybridized ZnO showed the same absorbance edge with the pure ZnO, but extended the absorbance to the visible region. The photocorrosion inhibition of ZnO by coupling with C₆₀ could be attributed to the reduced activation of surface oxygen atom. Since the interaction of C₆₀ and ZnO with the aid of a conjugative π -system, higher migration efficiency of photogenerated electrons could be produced at the interface of C₆₀ and ZnO, which brought about greater photocatalytic activity for C₆₀-hybridized ZnO. Long *et al.*⁸⁷ reported that the photocatalytic activity of C₆₀-incorporated TiO₂ nanorods under visible light irradiation was dramatically increased by a factor of approximately 3.3 and 2.7 when compared with that of pure TiO₂ nanorods and Degussa P25, respectively, which may be ascribed to an effective separation of the

photogenerated carriers with the introduction of C₆₀.

As one of the π -conjugated structure materials, the graphite-like carbon nitride (g-C₃N₄) has recently been investigated to exhibit a good photocatalytic activity for wastewater treatment under visible light irradiation.^{96,97} In comparison with the aforementioned π -conjugated structure, g-C₃N₄ is a soft polymer so that it can easily decorate on the surface of a photocatalyst, promoting the formation of core-shell structures. Sun *et al.*⁹⁶ synthesized g-C₃N₄-ZnO composite photocatalysts with different ZnO dosages in wt% by a simple calcination process, the absorption edge of which shifted toward the lower energy region and longer wavelengths in comparison with that of pure ZnO and g-C₃N₄. The remarkable photocatalytic activity of g-C₃N₄-ZnO composite for the photodegradation of methyl orange and p-nitrophenol under visible light irradiation could be ascribed mainly to the enhancement of electron-hole separations at the interface of ZnO and g-C₃N₄. Fu *et al.*⁹⁷ prepared g-C₃N₄-TiO₂ composite samples with different weight ratios by heating mixtures of melamine and commercial TiO₂. The samples with weight ratios g-C₃N₄: TiO₂ = 2.5 exhibited the highest adsorption capacity and enhanced visible light catalytic activity for degradation of methylene blue. The excited electrons on the surface of g-C₃N₄ could transfer easily to the TiO₂ CB *via* the well-built heterojunction, correspondingly inhibiting the recombination of photogenerated electron-hole pairs.

Conjugated polymer modification is one of the most promising methods for modifying TiO₂ to prepare visible-light-responsive photocatalysts. In the combined system of a conjugated polymer and a semiconductor, it is thermodynamically

possible to transfer the electrons from the conjugated polymer to the TiO₂ CB under the visible-light irradiation due to the fact that the conjugated polymer LUMO is energetically higher than the TiO₂ CB edge. Therefore, the occurrence of the interfacial charge transfer and separation between the conjugated polymer and the semiconductor guarantees the advanced photoresponse to visible light.⁸⁹ Li *et al.*⁹⁰ prepared a PANI-modified TiO₂ material using *in situ* chemical oxidative polymerization method, where the enhanced visible light photocatalytic activity in terms of the phenol degradation due to the synergetic effect amongst PANI and TiO₂. Meanwhile, Deng *et al.*⁹¹ and Luo *et al.*⁹⁸ observed the similar trend with regard to the enhancement of photocatalytic performances compared to the bare TiO₂ photocatalyst when probing the PPy-PANI-TiO₂ and polyisoprene modified TiO₂ system, respectively.

3.1.5. Other modification techniques

Montmorillonite has been employed to extend the light absorption region of photocatalysts, taking advantage of its several characters such as high crystallization, stronger cation exchange capacity, large specific surface area, and considerable active surface sites. For example, Li *et al.*⁹⁹ chose mesoporous montmorillonite as the supporting material for Sn²⁺-doped TiO₂, the absorption edges of the supported Sn²⁺-doped TiO₂ displayed a red shift and consequently exhibited higher visible-light catalytic activity than that of unloaded Sn²⁺-doped TiO₂. Zheng *et al.*¹⁰⁰ demonstrated that anatase TiO₂ films with dominant¹⁰¹ facets exhibited higher RhB degradation efficiency. Moreover, defect induced visible-light-responsive photocatalysts can also

be formed by introducing color centers within the material.¹⁰² To date, hydrogenation has been demonstrated as an effective route to induce defect in the surface layers of nanophase TiO₂. The disorder-engineered TiO₂ nanocrystals exhibited good solar-driven photocatalytic activities due to the marked extension of the optical absorption to the infrared range.¹⁰³ Another excellent candidate for the modification of photocatalysts is the integration of wide band-gap semiconductors with plasmonic metal nanocrystals, which could benefit from the increased concentration of photogenerated carriers and efficient utilization of visible light *via* plasmon-enhanced light absorption.¹⁰⁴

3.2. Novel visible-light-responsive photocatalysts

3.2.1. Multi-component oxide

Multi-component oxide as a new type of narrow band-gap photocatalyst with complex constitution has recently received extensive attention in the field of photocatalysis. Bismuth-based multi-component oxides have been under heavy investigations because of their great visible-light-responsive photocatalytic activity, which was proven to be superior to that of traditional TiO₂.¹⁰⁵ The narrow band-gap of bismuth-based multi-component oxides originates from the valence band consisting of Bi_{6s} and O_{2p} orbitals, which is more negative than that consisting of only O_{2p} ones (TiO₂).¹⁰⁶ Our recent studies on BiVO₄ indeed revealed that the BiVO₄ exhibited excellent visible-light or natural-sunlight photocatalytic activity.¹⁰⁷⁻¹¹⁰ In particular, the photocatalytic performances of BiVO₄ strongly rely on the shape configurations (as shown in Figure 2). Concerning with other bismuth-based

multi-component oxides, Dai *et al.*¹¹¹ demonstrated that Bi_2WO_6 hierarchical hollow spheres with an ultrahigh specific surface area possessed superior visible-light photocatalytic activity for the degradation of RhB over other morphological products. Very recently, Shang *et al.*¹¹² reported that $\text{Bi}_{24}\text{O}_{31}\text{Br}_{10}$ presented higher activity than that of Bi_2O_3 and BiOBr for the photocatalytic reduction of the Cr (VI) ions under visible light irradiation. Moreover, Bismuth titanate ($\text{Bi}_{12}\text{TiO}_{20}$) nanostructures with different morphologies were also synthesized, exhibiting advanced photocatalytic activity than that of traditional N-doped TiO_2 in terms of the degradation of acid orange 7.⁵¹

(Figure 2)

The photocatalytic properties of other multi-component oxides towards the degradation of organic contaminants under visible-light irradiation have been investigated. In one study, Ag_3PO_4 nanoparticles were synthesized by an ion-exchange reaction and nearly 80% of Cr (VI) ions were removed after visible-light irradiation in Ag_3PO_4 suspension, where the excellent photocatalytic reduction performance was attributed to the high separation efficiency of photogenerated charges.²⁸ Another study was concerned with the synthesis of CaIn_2O_4 rods as well as the measurements regarding the MB degradation and toluene oxidation under visible-light irradiation.¹¹³ In particular, MIn_2O_4 (M = Ca, Sr and Ba) semiconductors was employed for the degradation of MB under visible light irradiation and the highest photocatalytic activity was obtained by using CaIn_2O_4 .¹¹⁴

3.2.2. Nanocomposites

There have been considerable efforts to seek novel photocatalysts that are capable of harvesting visible light. Amongst the semiconductors with potentially good photocatalytic activities, considerable attention has been given to nanocomposites with tunable band-gap, which offers an opportunity to extend the absorption wavelength from the UV- to visible-light region. Moreover, compared with a single phase semiconductor, composites could promote the generation and separation of photogenerated carriers, and hence dramatically enhance the photocatalytic activity. The intercalation of bismuth-based oxides, ZnSnO_3 , SmVO_4 , CeO_2 , Bi_2MoO_6 , $\text{Fe}_{0.01}\text{Ni}_{0.01}\text{Zn}_{0.98}\text{O}$ and ZnFe_2O_4 particles into mesoporous materials such as graphene, $\text{g-C}_3\text{N}_4$, C_{60} , PANI, and multi-walled carbon nanotubes (MWCNTs) has been reported,^{33,35,115-121} where intercalation extended the absorption spectrum region. When these intercalated nanoparticles are excited by a band-gap irradiation, the photo-generated electrons and holes can be more efficiently utilized due to the high surface area to bulk ratio of the mesoporous structure. In the BiVO_4/RGO composites, the photo-generated e^- by sunlight irradiation in the CB of the BiVO_4 could be injected into RGO, while photo-generated holes remained in the VB of the BiVO_4 , directly oxidizing RhB molecules adsorbed on the surface of BiVO_4 . This charge-carrier separation was responsible for the improved photocatalytic activity.^{115,116} In our case, we prepared novel ZnSnO_3 hollow nanospheres formed at reduced graphene oxide (RGO), the as-prepared hybrid nanocomposites exhibited excellent photocatalytic activities for the decomposition of metronidazole under

visible light irradiation (Figure 3). The enhanced photocatalytic activity was due to the advanced adsorption efficiency of molecules, the reduction in the electron-hole recombination rate and enhanced visible light absorption within the hybrid nanocomposites by the introduction of RGO.³³

(Figure 3)

The novel g-C₃N₄/SmVO₄ composite photocatalyst with improved visible light photocatalytic activities for the RhB degradation was investigated by Li and colleagues.³⁵ The improvement originated from the synergetic effect of g-C₃N₄ and SmVO₄ based on the band position, the schematic illustration of electron-hole separation and transport at the visible-light-driven g-C₃N₄/SmVO₄ composite photocatalyst is shown in Figure 4. Channei *et al.*¹¹⁷ showed that Fe₃O₄/SiO₂/CeO₂ core-shell magnetic structures had higher photocatalytic degradation rate of formic and oxalic acid than that of bare CeO₂ under visible light. Zhang *et al.*¹¹⁸ reported the formation of Bi₂O₃/Bi₂SiO₅ nanoheterostructures within mesoporous SiO₂ microspheres, which exhibited excellent photocatalytic activities for the degradation of both acetaldehyde and bisphenol A under simulated solar light irradiation. The high photocatalytic efficiency was due to the efficiency charges separation stemming from a heterostructure junction effect. The C₆₀ modified Bi₂MoO₆ photocatalyst showed a high photocatalytic activity in the reduction of bromate ions under visible light irradiation.¹¹⁹ The enhanced photocatalytic activity maybe closely attributed to the interaction between Bi₂MoO₆ and C₆₀ which increased the photo-generated electron

mobility in Bi_2MoO_6 , C_{60} could effectively transfer the photoelectrons from CB of Bi_2MoO_6 after being illuminated under visible light irradiation. Kant *et al.*¹²⁰ synthesized $\text{Fe}_{0.01}\text{Ni}_{0.01}\text{Zn}_{0.98}\text{O}/\text{PANI}$ composite by *in situ* free radical polymerization method. Optical and photocatalytic studies revealed that the formation of composite further enhanced visible light absorption and photodegradation efficiency against MB under visible light irradiation. MWCNTs have potential for the fabrication of a novel nanocomposite due to its special aperture structure, high aspect ratio and large electron storage capacity. $\text{ZnFe}_2\text{O}_4/\text{MWCNTs}$ composite has been found suitable visible-light-responsive catalyst for the degradation of RhB.¹²¹ High-quality CuSe/ZnSe flower-like nanocomposites were fabricated as a visible-light-responsive photocatalyst through utilizing p-n junction effect and band gap engineering. The 8 wt% CuSe/ZnSe sample exhibited over 4 times and 2.5 times degradation ratio for both MO and MB than that of the pure ZnSe sample, respectively. The improvement was attributed to the effective separation of photogenerated carriers by the direct initiated interfacial charge transfer from the VB of ZnSe to CuSe, resulting in the reduction of CuSe to Cu_2Se .¹²²

(Figure 4)

3.2.3. Other emerging visible-light-responsive photocatalysts

$\text{ZrO}_2/\text{Dy}_2\text{O}_3$ materials with tunable compositions were synthesized and exhibited good photocatalytic degradation performances over both RhB and MB under visible light irradiation, which resulted from the special defect structure, small crystal size,

and large specific surface area.¹²³ $\text{Bi}_2\text{Mo}_x\text{W}_{1-x}$ ($x = 0-1$) solid solutions exhibited high photocatalytic activity for the degradation of RhB under visible light, which was mainly attributed to the special structure of solid solution and the lower energy band-gap.¹²⁴ The catalytic chemistry of polyoxometalates in promoting environmentally friendly photocatalytic process has also attracted considerable attention, examples are including the novel $\text{Ba}_4(\text{SiW}_4^{\text{V}}\text{W}_8^{\text{VI}}\text{O}_{40})\cdot\text{H}_2\text{O}$ ¹²⁵ and Bi^{3+} -doped NaTaO_3 powdered material.¹²⁶ Moreover, it has been shown that immobilizing palladium phthalocyaninesulfonate (PdPcS) integrated onto the FDU-15 mesopolymer provided a number of diamino groups inside the mesopores, which could be advantageous for the excellent visible light photocatalytic activity and reusability.¹²⁷

3.3. Unique features of visible-light-responsive photocatalysts

A photocatalysis process can be defined as a photo-induced reaction on the basis of semiconductor materials, which involves transforming light into other forms of energy. In a visible-light-responsive photocatalytic system, three key features should be considered. The first is the electronic structure, which determines the optical properties and band structure of the photocatalysts. The semiconductor should have the ability of absorbing visible light and the band-gap needs to be narrow enough to be excited by visible-light photons. The second key feature is the crystallinity, the high crystallinity means less crystalline defects, which would be beneficial to lowering the e^-h^+ recombination rate. The final key feature is the surface character, which usually exerts a critical effect on surface chemical reactions such as oxidation

by photo-generated holes and reduction by photo-generated electrons. The use of visible-light-responsive photocatalysts to introduce suitable physicochemical property is extremely common.

3.3.1. Optical properties and band structure

The optical property of probed photocatalysts is one of the crucial factors to predict their photocatalytic performance. The UV-vis spectrum can elucidate that the outer electrons of atoms absorb radiant energy and undergo transitions to higher energy levels, exhibiting special features in the spectrum in the absorption region. Light irradiation provides the photons required for the electron transfer from valence band to conduction band of the photocatalyst.¹²⁸ Both light intensity and wavelength are important due to the fact that (i) the overall energy input to a photocatalytic process relies upon the light intensity and (ii) the energy of a photon is related to light wavelength. In addition, if a highly concentrated pollutant solution is used, the chance of direct light absorption by the catalyst is low, therefore giving rise to retarded catalytic activity. Soltani *et al.*¹²⁹ managed to extend the light absorption of ZnS and CdS nanoparticles to the visible region, where the stability of such materials against photo-corrosion as well as the degradation efficiency of dyes were improved. Tan *et al.*¹³⁰ demonstrated that Sm was partially introduced in the crystal lattice of ZnIn₂S₄ microspheres to produce a doping energy level, which promoted the separation of photo-induced electron-hole pairs and enhanced the absorption of visible light, leading to higher photodegradation efficiency of RhB under visible light irradiation.

Herein another important point is that photo-absorption and e^-h^+ generation are

inextricably linked. Since the ability of a photocatalyst is exclusively governed by its band structure, from the thermodynamic point of view, estimation of the potential of the VB top and CB bottom is essential to predict the possibility in driving a photocatalytic reaction. A general way for such estimation involves measurements of optical absorption property, and the optical band-gap can be estimated using the following equation:

$$Ah\nu = C(h\nu - E_g)^n \quad (3.9)$$

where C denotes a constant, A , E_g , h , and ν represents the absorption coefficient, the band-gap energy, Planck constant, and the incident light frequency, respectively. The band-gap energy (E_g) of the photocatalysts can be estimated from a plot depicting $(Ah\nu)^{1/n}$ versus $h\nu$. The constant n is 1/2, 3/2, 2 or 3 for direct transition, forbidden direct transition, indirect transition or forbidden indirect transition, respectively, where the forbidden direct or indirect transition has always been neglected. Moreover, feasible e^- and/or h^+ transfer from one component unit to another with proper band edge positions can greatly suppress the e^- - h^+ recombination probability and increase the lifetime of charge carriers, thus promoting the photocatalytic efficiency. In this regard, Kanhere *et al.*¹²⁶ reported that the optical properties obtained by the band structure calculations were in good agreement with the experimentally observed absorption spectra.

The photocatalytic removal efficiency of MO, RhB and MB was enhanced under both simulated solar light and visible light irradiation when the photonic band gaps of the TiO₂ photonic crystals were matched well with the absorption peaks of the

corresponding dyes. The improvement could be attributed to the intensified dye sensitization as a result of slow photon effect on the edges of the photonic band gaps.¹³¹ When commercial TiO₂ crystals coupled with a trace amount of narrow-band-gap Ag₂CO₃, the photocatalytic degradation activity under visible light irradiation of the composite was enhanced due to the promoted visible light absorption and the suppressed recombination rate of e⁻/h⁺ pairs.¹³² It was also demonstrated that the optical properties of the Cu₂PO₄OH hierarchical superstructures were strongly related to their morphologies and the size of the assembled crystallites, where the walnut-shaped morphology exhibited the best photocatalytic performance due to the excellent visible light absorption ability as well as a high BET surface area.¹³³

3.3.2. Crystallinity

Photocatalysts are usually inorganic solid materials which are often crystals. The crystallinity often bonds together with other features such as optical properties, electronic structures and photocatalytic performance. It is well known that BiVO₄ can exist in three crystalline phases, namely, zircon tetragonal (*zt*BiVO₄), scheelite tetragonal (*st*BiVO₄) and monoclinic clinobisvanite (*m*BiVO₄). Ding *et al.*¹³⁴ investigated the electronic structures and optical properties of the three crystalline phases of BiVO₄ by DFT calculations. The results showed that *zt*BiVO₄ was a semiconductor with a direct minimum band gap, which was obviously larger than that of indirect band gap semiconductors *st*BiVO₄ and *m*BiVO₄. The zircon tetragonal phase also exhibited most powerful oxidation and reduction ability, but the weakest

visible light absorption ability, whilst the other two phases showed similar band edge positions and absorption spectra. *ztBiVO₄* exhibited distinct electronic properties due to the shortest Bi-O bond results in the strongest covalent interaction between Bi and O, whilst the electronic structures, distributions of density of states, atomic populations, the atomic charges of *stBiVO₄* and *mBiVO₄* were quite similar. It was worthwhile to note that *mBiVO₄* had dominant photocatalytic activity compared with the other crystalline phases due to its excellent performance in generation and separation of photoinduced carriers. TiO₂ has three crystalline polymorphs in nature: brookite, rutile and anatase, where TiO₆ octahedral with some extent of distortion are connected by shared corners and/or edges determining the crystal structure. Among them, anatase TiO₂ usually shows greatly superior photoactivity to rutile and brookite. The packing density discrepancy between anatase and rutile/brookite affects the bulk diffusion capability of carriers, which is another important factor in controlling the photoactivity in addition to the stronger adsorptive affinity of anatase for organic molecules.⁴⁴ The mixtures of anatase/rutile, brookite/rutile and anatase/brookite (anatase/rutile in particular) result in synergistic photocatalytic effects on charge-carrier transfer by forming an intimate contact in the interface of two phases. Moreover, some dopants can exist as their oxide clusters instead of atoms within the surface/subsurface of doped matrices due to the differences in crystal structure and crystal nucleation ability between dopants and matrices. In addition, doping-induced phase transformations of photocatalysts are also sensitive to how pristine the photocatalysts' crystal structures are.¹³⁵

3.3.3. Surface features

One of the representative cases for kinetics of reactions occurring on the photocatalyst surface is the so-called “surface reaction limited” process. Under this condition, surface adsorption is kept in equilibrium during the reaction and the overall rate coincides with the rate of reaction occurring on the surface. Therefore, in addition to the basic requirements of electronic structure for the semiconductor in the photocatalytic systems, a favorable interface structure is vital in promoting interface transfer of carriers *via* different pathways. As we all know, the adsorption ability of a photocatalyst is one of the essential factors to influence the photo-activity because it is beneficial to the transfer of charge carriers between the radical ions of pollutant and semiconductor. It has been demonstrated that the photocatalytic degradation efficiency relied greatly on the adsorption behavior between target pollutant molecules and photocatalyst, and the adsorption of pollutant molecules on catalyst can significantly improve the degradation efficiency.¹³⁶ It is of great importance to investigate the adsorption process of pollutants on the photocatalyst surface to clarify the mechanism of photocatalytic reactions, which in turn, could facilitate their applications in water purification. The surface of photocatalysts are positively charged in acidic solutions and negatively charged in alkaline solutions.¹²⁹ The photocatalysts with different surface charges would exhibit a highly selective adsorption of charged targeted pollutants and a molecular recognitive photocatalytic performance *via* the electrostatic attraction or repulsion.¹³⁷ The adsorption ability is also affected by the predominant atomic state for the electronegativity of the exposed facets.¹³⁰ For

example, Tan *et al.*¹³⁰ found that hexagonal ZnIn₂S₄ with dominant {0001} facets exhibit high adsorption ability toward cationic RhB, whilst weak adsorption ability toward anionic MO dye molecules, implying that the exposed {0001} facets of hexagonal ZnIn₂S₄ microspheres were beneficial to adsorbing cationic dye molecules. Further study indicated that the surface electronegativity of the prepared ZnIn₂S₄ was the primary factor for the higher adsorption of RhB and the exposed S atom of the {0001} facets was the primary factor for the improved photocatalytic efficiency of hexagonal ZnIn₂S₄.

The redox potential of the reaction substrates, which adsorbed on the surface varies to the amount of adsorbed substrates and the surface chemical structure, depends more directly on the specific surface area. Table 1 summarizes the various preparation methods of visible-light-responsive photocatalysts with various Brunauer-Emmett-Teller (BET) surface areas. In general, the high surface area to volume ratio of photocatalysts appears to be an important parameter for designing and engineering photocatalytic materials. For example, Dai *et al.*⁶¹ prepared C-doped Bi₂O₃ with a porous structure by a simply calcination of Bi(NO₃)₃·5H₂O in glycol solution. The porous materials possess larger specific surface area, which contributed to more possible reaction sites on the photocatalyst surface, as well as facilitated the rapid diffusion of ions and molecules within the material, resulting in the higher photocatalytic activity. Kim *et al.*¹³⁸ reported that the dye degradation performance was further markedly enhanced under visible light irradiation with a dramatic increase in the BET surface area, with an order of 2D BiOCl (5.5 m²·g⁻¹) < 3D BiOCl (16.8

$\text{m}^2\cdot\text{g}^{-1}$) \ll $\text{BiOCl}_{0.6}\text{I}_{0.4}$ ($46.6 \text{ m}^2\cdot\text{g}^{-1}$). Such investigations indicate that the specific surface area plays an important role in the photo-degradation of the pollutant. Besides, the photocatalytic performances are not solely related to the surface area but also influenced by the surface charge, crystal facets, band structure, and optical properties, etc. For instance, Owing to the change of surface charge and the newly created recombination center with the Ag-loading, the photocatalytic degradation performance of the Ag-doped $\text{BiOCl}_{0.6}\text{I}_{0.4}$ was dramatically reduced upon loading with small amounts of Ag, although the BET surface area increased from $46.6 \text{ m}^2\cdot\text{g}^{-1}$ to $49.1 \text{ m}^2\cdot\text{g}^{-1}$ with the Ag-loading. Our recent study on the sunlight photocatalytic performances of BiVO_4 also found that the BET surface area was not the only factor in influencing the photocatalytic activities.¹⁰⁷

Apart from the crystal facet and electronic structures, the existence of surface defects on photocatalysts stays another important factor affecting its photocatalytic performance. The roles of the defects played in the adsorption and surface reactivity have been acknowledged and extensively characterized by various techniques.^{132,139,140} Yu *et al.*¹³² revealed that more surface hydroxyl groups over the $\text{Ag}_2\text{CO}_3/\text{TiO}_2$ composite could react with the photo-generated h^+ and produce $\cdot\text{OH}$ radicals to decompose the dye. Zhang *et al.*¹³⁹ demonstrated that the visible hydroxyl groups indicated the existence of surface defects on ZnO nanorods and the existence of surface defects played a positive role in the photocatalytic activity of ZnO nanorods. The photo-generated holes could be trapped by surface defects and the separation of photo-generated e^-/h^+ pairs was facilitated. Moreover, the

photo-generated holes trapped by surface defects were readily to react with electron donors and the photocatalytic reaction could be greatly promoted; this was the reason why ZnO nanorods with surface defects showed significantly higher photocatalytic performances. Bai *et al.*¹⁴⁰ showed that the ZnO_{1-x} with surface oxygen defect could be excited by visible light due to the narrowing energy band-gap, resulting from the generation of the surface defect level induced by surface oxygen-defect states. The surface defects may serve as adsorption sites as well as charge carrier traps where the charge transfers to the adsorbed species and prevents the e⁻/h⁺ recombination. However, TaON nanoparticles with lower surface reduction defect sites exhibited enhanced photocatalytic performance for the mineralization of phenol and its chloro-derivatives in an aqueous phase under visible light irradiation.³⁷ A possible interpretation of this phenomenon is that the photocatalytic performance would not be governed by a single feature. In a diverse photocatalysis system, combined photocatalysts in different combinations and ratios could provide varied results depending upon the conditions used.

4. Application of visible-light-responsive photocatalyst in water treatment

Visible-light-responsive photocatalysts are expected to play an important role in tackling the growing concern over the water contamination, which is of great significance in alleviating the increasingly serious water resource crisis. The photocatalysis route itself holds many advantages such as strong oxidation power, moderate operation temperature and green-chemistry related procedures, offering a tantalizing route to meet the global challenges associated with the environment,

energy and sustainability with the aid of abundant sunlight resources. Visible-light-responsive photocatalysts have been widely used for the treatment of inorganic, organic, and biological contaminated water. In this section the main applications of visible-light-responsive photocatalysts in water treatment are briefly summarized, and it is worth-noting that most applications discussed here are still in the stage of laboratory research.

4.1. Photocatalytic degradation of organic pollutants

In most cases, different types of dyes are studied as model compounds for the photocatalytic degradation of large organic molecules in water treatment. Organic dyes are often used in textile, printing, and photographic industries, from which a sizable fraction of dyes is wasted in the dyeing process and released into the effluent water streams. In general, the presence of low concentrations of dyes in effluent streams seriously affects the nature of water, and is difficult to be biodegraded or oxidized with the aid of chemicals. Therefore, appreciable efforts have been made to develop photocatalysts to degrade dyes in aqueous solutions under visible light.¹⁴¹⁻¹⁴³ Bismuth titanate ($\text{Bi}_{12}\text{TiO}_{20}$) nanostructures with different morphologies were used to photocatalytically remove acid orange 7 under visible light irradiation, showing that $\text{Bi}_{12}\text{TiO}_{20}$ had higher photocatalytic activity than that of traditional N-doped TiO_2 ; in this regard, BET surface area played an important role in the reaction efficiency, while the crystallinity of the samples was another important factor that could also boost the photocatalytic performances.⁵¹ Photosensitization of photocatalyst by dyes has also been used for the visible photo-degradation and mineralization of dye pollutants. Li *et*

*al.*¹⁴¹ initiated a comparison study of dye photodegradation over TiO₂ and ZnO, where the microscale ZnO exhibited much higher visible photocatalytic activity than that of P25 due to the higher photosensitization efficiency of electron transfer from an excited dye to the CB of the microscale ZnO than that of P25. The better crystallinity and lower defects of the microscale ZnO than that of the nanosized ZnO could result in a better photostability. TiO₂-modified ZnO was developed as a novel light-to-electricity conversion device, which was proven to be a promising candidate for the photocatalytic removal of dye pollutants as well as a renewable energy source.

Pharmaceutical and personal care products (PPCPs) have recently been considered as emerging contaminants, which are extraordinarily diverse groups of chemicals used in prescription and nonprescription drugs, human health and cosmetic care, veterinary medicine, and agricultural practice.¹⁴⁴ Specific PPCPs may cause ecological harm, such as endocrine disruption and antimicrobial resistance, thus some of PPCPs have been classified as the 'priority pollutants' by both the US Environmental Protection Agency and the European Union Water Framework Directive. PPCPs have frequently been studied with respect to the domain of environmental protection because of its toxicity and non-biodegradability. To date, visible-light photocatalytic degradation technique has been considered as a promising approach for the environmentally-friendly decomposition of PPCPs with high efficiency, cost effectiveness, ease of operation *etc.* For example, An and Zhou¹⁴⁵ employed a new combined catalyst copper-plating iron doped Cu₂O (FeCu/Cu₂O) to degrade a mixture of five commonly used PPCPs (sulfamethoxazole, oxytetracyclin,

paracetamol, aspirin, and triclosan) under visible light irradiation. Compared with the Fe/C inner micro-circuit, the electric currents flowing between Cu and Fe increased the speed of anodic Fe dissolution. Cu_2O could accelerate the PPCP degradation processes under visible light irradiation due to the photochemical properties. Moreover, the increased dissolved oxygen concentration in the solution by shaking not only preconditioned the photo-catalysis reaction, but also set the stage for Fe reduction. Zhao *et al.*¹⁴⁶ investigated the photochemical degradation of the antibiotic oxytetracycline (OTC) with nitrogen and fluorine doped titanium dioxide (NF-TiO₂) film at different pH values in aqueous solutions under visible and solar light irradiation. The kinetics and mechanism during the photolytic and photocatalytic degradation of OTC were intensively studied. The photochemical degradation of OTC with NF-TiO₂ film could occur *via* a number of competing reaction processes, such as direct photolytic degradation as shown in Figure 5; the electrons and holes can be separated by the excited NF-TiO₂ under light irradiation, followed by the fact that a series of active redox species were produced by a series of reactions, leading to the oxidative-reductive degradation of OTC.

(Figure 5)

The phenolic compounds might cause various diseases including cancer, angiocardopathy and gastroenterology *etc.*, even at very low concentrations, which represent a typical family of organic pollutants widely present in wastewater coming from petrol, coal, and other chemical industries.¹⁴⁷ Most phenolic compounds are

usually difficult to be mineralized by a biodegradation method due to the stable benzene ring and its recalcitrant nature. However, such compounds have been reported to be effectively degraded by visible-light-responsive photocatalyst.^{30,79,127,37,147} Li and colleagues¹⁴⁷ synthesized a novel layered perovskite crystal La_2NiO_4 photocatalyst with high activity for mineralizing 4-chlorophenol under visible light irradiation. Firstly, the 4-chlorophenol ionized into anions and donated electrons to La_2NiO_4 due to the positively charged surface. Then, the electrons could react with dissolved O_2 to produce $\cdot\text{O}_2^-$ radicals, followed by reacted with H^+ to form $\cdot\text{OH}$ radicals, which could oxidize 4-chlorophenol into CO_2 , leading to complete degradation. Other organic pollutions such as benzyl alcohol,¹⁴⁸ methanol,¹⁴⁹ benzyl amine,¹⁵⁰ hydroxytyrosol,¹⁵¹ and benzene¹⁵² in the aqueous solutions have also been reported to be efficiently degraded by visible-light induced photocatalytic.

4.2. Photocatalytic degradation of inorganic pollutants

The presence of inorganic impurities such as residual ions and acids in the water matrix has distinctive effects towards the water ecological environment. Some of them are highly toxic to most of the living organisms when their concentration levels are higher than a certain value. Hexavalent chromium (Cr(VI)) is a carcinogenic and mutagenic pollutant which is frequently found in wastewater, possibly stemming from the pigment production, metal plating and leather tanning, *etc.* The visible-light induced photocatalytic reduction of aqueous Cr(VI) has received much attention recently due to its low cost and high efficiency without secondary pollution.^{153,154} For

instance, the synthesized SnIn_4S_8 particles with flower-like nanostructure could exhibit excellent photocatalytic reduction efficiency of aqueous Cr(VI) (~97%) and good photocatalytic stability.¹⁵³ The strong absorption in visible-light region, large surface area and excellent charge separation characteristics of SnIn_4S_8 were responsible for the promising removal performance. The mechanism for Cr(VI) removal from water by SnIn_4S_8 is shown in Figure 6. The photo-generated electrons in the VB of SnIn_4S_8 could be excited to the CB while the holes were generated in the VB. Subsequently, a portion of the photo-generated e^-h^+ pairs migrated to the surface of the SnIn_4S_8 and participated in the redox reaction. The photo-generated e^- reduced the adsorbed Cr(VI) to Cr(III) , meanwhile the h^+ enabled the oxidization of water to O_2 . By this mean, the photocatalytic reduction of Cr(VI) coupling with the synergistic effect of photo-degradation of bisphenol A in aqueous solution were also achieved by using $\text{Bi}_2\text{O}_3/\text{TiO}_2$ under visible-light irradiation.¹⁵⁴

(Figure 6)

4.3. Photocatalytic disinfection of biological pollutants

The different types of microbes (bacteria, viruses, fungi, algae, plankton, etc.) presented in wastewater are harmful to cause various diseases.¹⁵⁵ Over the past decades, visible light activated photocatalytic disinfection of water has received significant attention with research focus moving from laboratory studies to potential applications.^{156,157} For example, dye-sensitized TiO_2 thin film was used to photocatalytic disinfection of phytopathogenic bacteria under visible light irradiation.

The inhibition rates of *Erwinia carotovora subsp. carotovora* 3, *Enterobacter cloacae* SM1 and *E. carotovora subsp. carotovora* 7 that could induce severe soft/basal rot disease in vegetable crops were higher than 90%. The results indicated that the visible-light-responsive dye-sensitized TiO₂ thin film had the potential for direct application to plant protection in water systems.¹⁵⁶ Visible-light activated palladium-modified nitrogen-doped titanium oxide (TiON/PdO) photocatalyst was demonstrated with good visible light adsorption and superior efficient photocatalytic disinfection effect on Fungi *Fusarium graminearum* macroconidia. The disinfection effect benefitted from the strong adsorption of TiON/PdO photocatalyst onto the *Fusarium graminearum* macroconidia surface due to their opposite surface charges. The photocatalytic disinfection mechanism of TiON/PdO photocatalyst on the *Fusarium graminearum* macroconidia is displayed in Figure 7, which was attributed to their cell wall/membrane damage caused by the attack from reactive oxygen species (ROSs), while a breakage of their cell structure was not necessary for their loss of viability.¹⁵⁷

(Figure 7)

5. Conclusion and perspectives

Visible-light-responsive photocatalysis for water and wastewater treatment is gaining momentum globally and presenting great opportunities to revolutionize water and wastewater treatment due to the unique features. In this review, we have extensively reviewed the current progress in heterogeneous photocatalytic water

treatment using visible-light-responsive photocatalysts. The fundamentals of heterogeneous photocatalysis and regulatory mechanism of visible-light-responsive photocatalysis, as well as the unique features of visible-light-responsive photocatalysts have been briefly discussed. In order to extend the optical response of photocatalyst into the visible region, a variety of methods such as modification of traditional photocatalysts *via* doping, dye sensitization, forming a heterostructure, coupled with π -conjugated structure, and exploration of novel multi-component oxides and nanocomposites with visible light responses have been developed. These photocatalysts have been widely used for the degradation of inorganic and organic pollutants, as well as photocatalytic disinfection. Therefore, these results are promising for further development of sustainable environmental remediation technologies, based on photocatalytic redox reactions driven by visible light as a renewable source of energy.

Although steady progress in heterogeneous photocatalytic water treatment by using visible-light-responsive photocatalysts has been achieved,¹⁵⁸ studies in this field are still at the immature stage and further developments are required. The challenges faced by water treatment with visible-light-responsive photocatalyst are important, but many of which are perhaps only temporary, including high cost, technical hurdles, and potential environmental and human risk. In order to promote the feasibility of visible-light-responsive photocatalytic water treatment technology in the near future, several key technical constraints ranging from catalyst development to reactor design and process optimization have to be addressed, including the following aspects:

(i) Improving the efficiency and photo-stability of the visible-light-responsive photocatalyst. The performance of visible-light responsive photocatalyst is currently limited by the physicochemical properties of these materials. For example, among the modification methods, though dye sensitization has been able to extend the adsorption light wavelength to visible-light range and improve the activity of traditional photocatalysts under visible light, the usage of such photocatalytic materials is still limited due to issues regarding the dissolution and degradation of dyes, which retards their photocatalysis applications. Therefore, a more careful design of the functional photocatalyst is required to obtain suitable physicochemical properties of materials.

(ii) Devising photocatalyst immobilization strategy to provide a cost-effective solid-liquid separation. One detrimental limitation at the current stage is running-out of the catalyst during the photocatalytic process, which jeopardizes the regeneration of the catalysts and poses adverse impacts on the environments due to the leakage of the photocatalyst. Immobilized photocatalytic systems can avoid problems associated with catalyst recovery and agglomeration, as well as minimizing the scale of the reactor.

(iii) Designing effective photoreactor for the full utilization of solar energy to reduce the electricity costs. The implementation of photocatalytic processes at an industrial level requires the design of suitable photoreactors, where a proper design and build-up of such devices would be helpful to better harvest solar energy, accommodate the photocatalysts and reactants, as well as collect the reaction products.

(iv) Establishing a globally experimental database regarding the information of the try-out photocatalysts, including the types of catalyst materials, preparation routes, modifications, photocatalytic reaction environments and activity, etc. Such database should be accessed to avoid any repeated, unnecessary work and guide the development of innovative catalysts. In order to obtain desirable photo-degradation efficiency, combining different techniques and approaches might be indispensable. In this regard, a database detailing the fabrication and usage of the existing photocatalysts needs to be established, since plenty of nanostructured materials have already been used in the visible-light-responsive photocatalysis. The accumulation of a large amount of theoretical and modelling work is also useful and imperative in the quest to foster a deep understanding of the preparation, properties and performance of photocatalysts and their optimization for water treatment. Multi-technology integration will provide a bright prospect for water treatment and energy-related issues using visible-light-responsive photocatalysts with advanced efficiency and good robustness.

Acknowledgements

The authors are grateful for the financial support from the Key Science and Technology Program of Henan Province, PR China (Grant Nos. 122102310486 and 132102210129), the Basic Scientific and Technological Frontier Project of Henan Province, PR China (Grant Nos. 102300410098, 132330410138, and 122300410293). The authors also would like to thank the Innovation Scientists and Technicians Troop Construction Projects of Henan Province, the Plan for Scientific Innovation Talent of

Henan Province (Grant No. 134200510014), the Fostering Foundation of Henan Normal University for the Author of National Excellent Ph.D. Dissertation, PR China (Grant No. 01333900011), and the National Natural Science Foundation of China (Grants No. 21477034).

References

- 1 J. Qu and M. Fan, *Crit. Rev. Env. Sci. Tec.*, 2010, **40**, 519-560.
- 2 X. Zhou, Y. Li and Y. Zhao, *RSC Adv.*, 2014, **30**, 15620-15629.
- 3 V. K. Gupta, I. Ali, T. A. Saleh, A. Nayak and S. Agarwal, *RSC Adv.*, 2012, **2**, 6380-6388.
- 4 J. Sun, B. Zhang, R. Sun, Y. Li and J. Wu, *Int. J. Environ. Pollut.*, 2009, **38**, 81-87.
- 5 S. Sun, C. Li, J. Sun, S. Shi, M. Fan and Q. Zhou, *J. Hazard. Mater.*, 2009, **161**, 1052-1057.
- 6 J. Sun, S. Sun, M. Fan, H. Guo, Y. Lee and R. Sun, *J. Hazard. Mater.*, 2008, **153**, 187-193.
- 7 O. Ganzenko, D. Huguenot, E. D. van Hullebusch, G. Esposito and M. A. Oturan, *Environ. Sci. Pollut. R.*, 2014, **21**, 8493-8524.
- 8 S. Ray, M. Takafuji and H. Ihara, *RSC Adv.* 2013, **3**, 23664-23672.
- 9 M. Tanveer and G. T. Guyer, *Renew. Sust. Energ. Rev.*, 2013, **24**, 534-543.
- 10 L. Yang, S. Dong, J. Sun, J. Feng, Q. Wu and S. Sun, *J. Hazard. Mater.*, 2010, **179**, 438-443.
- 11 P. Fageria, S. Gangopadhyay and S. Pande, *RSC Adv.* 2014, **4**, 24962-24972.

- 12 S. Balachandran, S. G. Praveen, R. Velmurugan and M. Swaminathan, *RSC Adv.* 2014, **4**, 4353-4362.
- 13 Y.C. Chang, *RSC Adv.* 2014, **4**, 20273-20280.
- 14 L. G. Devi and R. Kavitha, *Appl. Catal. B: Environ.*, 2013, **140**, 559-587.
- 15 D. Kanakaraju, B. D. Glass and M. Oelgemoeller, *Environ. Chem. Lett.*, 2014, **12**, 27-47.
- 16 A. Rey, P. Garcia-Munoz, M. D. Hernandez-Alonso, E. Mena, S. Garcia-Rodriguez and F. J. Beltran, *Appl. Catal. B: Environ.*, 2014, **154**, 274-284.
- 17 J. Sun, L. Qiao, S. Sun and G. Wang, *J. Hazard. Mater.*, 2008, **155**, 312-319.
- 18 Z. Li, Y. Fang and S. Xu, *Mater. Lett.*, 2013, **93**, 345-348.
- 19 L. Z. Qin, H. Liang, B. Liao, A. D. Liu, X. Y. Wu and J. Sun, *Nucl. Instrum. Meth. B.*, 2013, **307**, 385-390.
- 20 Y. Min, K. Zhang, Y. Chen and Y. Zhang, *Chem. Eng. J.*, 2011, **175**, 76-83.
- 21 Q. Li, L. Zong, Y. Xing, X. Wang, L. Yu and J. Yang, *Sci. Adv. Mater.*, 2013, **5**, 1316-1322.
- 22 B. Ohtani, *J. Photoch. Photobio. C.*, 2010, **11**, 157-178.
- 23 C. Mondal, M. Ganguly, J. Pal, A. Roy, J. Jana and T. Pal, *Langmuir*, 2014, **30**, 4157-4164.
- 24 W. Wang, J. Wang, Z. Wang, X. Wei, L. Liu, Q. Ren, W. Gao, Y. Liang and H. Shi, *Dalton. Trans.*, 2014, **43**, 6735-6743.
- 25 S. Zhang, *Ceram. Int.*, 2014, **40**, 4553-4557.
- 26 Z. Li, S. Yang, J. Zhou, D. Li, X. Zhou, C. Ge and Y. Fang, *Chem. Eng. J.*, 2014,

- 241, 344-351.
- 27 S. Wang, D. Li, C. Sun, S. Yang, Y. Guan and H. He, *J. Mol. Catal. A-Chem.*, 2014, **383**, 128-136.
- 28 H. Huang, Y. Feng, J. Zhou, G. Li and K. Dai, *Desalin. Water Treat.*, 2013, **51**, 7236-7240.
- 29 H. Cheng, B. Huang and Y. Dai, *Nanoscale*, 2014, **6**, 2009-2026.
- 30 J. Sheng, X. Li and Y. Xu, *Acs Catal.*, 2014, **4**, 732-737.
- 31 Y. S. Xu, Y. X. Yu and W. D. Zhang, *J. Nanosci. Nanotechnol.*, 2014, **14**, 6800-6808.
- 32 U. M. Garcia-Perez, A. Martinez-de la Cruz and J. Peral, *Electrochim. Acta*, 2012, **81**, 227-232.
- 33 S. Dong, J. Sun, Y. Li, C. Yu, Y. Li and J. Sun, *Appl. Catal. B: Environ.*, 2014, **144**, 386-393.
- 34 M. Shang, W. Wang, L. Zhou, S. Sun and W. Yin, *J. Hazard. Mater.*, 2009, **172**, 338-344.
- 35 T. Li, L. Zhao, Y. He, J. Cai, M. Luo and J. Lin, *Appl. Catal. B: Environ.*, 2013, **129**, 255-263.
- 36 L. Armelao, D. Barreca, G. Bottaro, A. Gasparotto, C. Maccato, C. Maragno, E. Tondello, U. L. Stangar, M. Bergant and D. Mahne, *Nanotechnology*, 2007, **18**, 375709.
- 37 Y. Chen, S. Liang, L. Wen, W. Wu, R. Yuan, X. Wang and L. Wu, *Phys. Chem. Chem. Phys.*, 2013, **15**, 12742-12747.

- 38 D. Barreca, A. P. Ferrucci, A. Gasparotto, C. Maccato, C. Maragno and E. Tondello, *Chem. Vapor Depos.*, 2007, **13**, 618-625.
- 39 L. Armelao, D. Barreca, G. Bottaro, A. Gasparotto, C. Maccato, E. Tondello, O. I. Lebedev, S. Turner, G. Van Tendeloo, C. Sada and U L. Stangar, *Chemphyschem*, 2009, **10**, 3249-3259.
- 40 G. Carraro, R. Sugrañez, C. Maccato, A. Gasparotto, D. Barreca, C. Sada, M. Cruz-Yusta and L. Sánchez, *Thin Solid Films*, 2014, **564**, 121-127.
- 41 A. Abd Aziz, C. K. Cheng, S. Ibrahim, M. Matheswaran and P. Saravanan, *Chem. Eng. J.*, 2012, **183**, 349-356.
- 42 M. N. Chong, B. Jin, C. W. K. Chow and C. Saint, *Water. Res.*, 2010, **44**, 2997-3027.
- 43 E. Casbeer, V. K. Sharma and X. Z. Li, *Sep. Purif. Technol.*, 2012, **87**, 1-14.
- 44 Y. Qu and X. Duan, *Chem. Soc. Rev.*, 2013, **42**, 2568-2580.
- 45 C. Chen, W. Ma and J. Zhao, *Chem. Soc. Rev.*, 2010, **39**, 4206-4219.
- 46 R. Abe, *J. Photoch. Photobio. C.*, 2010, **11**, 179-209.
- 47 K. Mori and H. Yamashita, *Phys. Chem. Chem. Phys.*, 2010, **12**, 14420-14432.
- 48 X. Qu, P. J. J. Alvarez and Q. Li, *Water. Res.*, 2013, **47**, 3931-3946.
- 49 X. G. Yan, L. Xu, W. Q. Huang, G. F. Huang, Z. M. Yang, S. Q. Zhan and J. P. Long, *Mater. Sci. Semicon. Process.*, 2014, **23**, 34-41.
- 50 L. Gu, J. Wang, Z. Zou and X. Han, *J. Hazard. Mater.*, 2014, **268**, 216-223.
- 51 X. Zhu, J. Zhang and F. Chen, *Chemosphere*, 2010, **78**, 1350-1355.
- 52 J. Sun, S. Dong, Y. Wang and S. Sun, *J. Hazard. Mater.*, 2009, **172**, 1520-1526.

- 53 J. Sun, Y. Wang, R. Sun and S. Dong, *Mater. Chem. Phys.*, 2009, **115**, 303-308.
- 54 R. Asahi, T. Morikawa, T. Ohwaki, K. Aoki and Y. Taga, *Science (New York, N.Y.)*, 2001, **293**, 269-271.
- 55 G. Liu, L. Wang, H. G. Yang, H.-M. Cheng and G. Q. Lu, *J. Mater. Chem.*, 2010, **20**, 831-843.
- 56 C. Di Valentin and G. Pacchioni, *Catal. Today*, 2013, **206**, 12-18.
- 57 W. J. Ong, L. L. Tan, S. P. Chai, S. T. Yong and A. R. Mohamed, *Nanoscale*, 2014, **6**, 1946-2008.
- 58 Y. Wang, C. Feng, M. Zhang, J. Yang and Z. Zhang, *Appl. Catal. B: Environ.*, 2010, **100**, 84-90.
- 59 B. Neumann, P. Bogdanoff, H. Tributsch, S. Sakthivel and H. Kisch, *J. Phys. Chem. B*, 2005, **109**, 16579-16586.
- 60 Y. J. Chen, G. Y. Jhan, G. L. Cai, C. S. Lin, M. S. Wong, S. C. Ke, H. H. Lo, C. L. Cheng and J. J. Shyue, *J. Vac. Sci. Technol. A.*, 2010, **28**, 779-782.
- 61 G. Dai, S. Liu and Y. Liang, *J. Alloy. Compd.*, 2014, **608**, 44-48.
- 62 M. Samadi, H. A. Shivaee, M. Zanetti, A. Pourjavadi and A. Moshfegh, *J. Mol. Catal. A: Chem.*, 2012, **359**, 42-48.
- 63 R. Leary and A. Westwood, *Carbon*, 2011, **49**, 741-772.
- 64 M. Pelaez, N. T. Nolan, S. C. Pillai, M. K. Seery, P. Falaras, A. G. Kontos, P. S. M. Dunlop, J. W. J. Hamilton, J. A. Byrne, K. O'Shea, M. H. Entezari and D. D. Dionysiou, *Appl. Catal. B: Environ.*, 2012, **125**, 331-349.
- 65 J. Li, J. Xu and J. Huang, *Cryst. Eng. Comm.*, 2014, **16**, 375-384.

- 66 B. K. Vijayan, N. M. Dimitrijevic, J. Wu and K. A. Gray, *J. Phys. Chem. C*, 2010, **114**, 21262-21269.
- 67 J. Sun, S. Dong, J. Feng, X. Yin and X. Zhao, *J. Mol. Catal. A: Chem.*, 2011, **335**, 145-150.
- 68 H. F. Moafi, M. A. Zanjanchi and A. F. Shojaie, *J. Nanosci. Nanotechnol.*, 2014, **14**, 7139-7150.
- 69 Y. C. Wu and L. S. Ju, *J. Alloy. Compd.*, 2014, **604**, 164-170.
- 70 H. Sun, G. Zhou, S. Liu, H. M. Ang, M. O. Tade and S. Wang, *Chem. Eng. J.*, 2013, **231**, 18-25.
- 71 J. Zhao, C. Chen and W. Ma, *Top. Catal.*, 2005, **35**, 269-278.
- 72 Z. Li, Y. Fang, X. Zhan and S. Xu, *J. Alloy. Compd.*, 2013, **564**, 138-142.
- 73 D. Chatterjee and S. Dasgupta, *J. Photoch. Photobio. C.*, 2005, **6**, 186-205.
- 74 J. Shang, F. Zhao, T. Zhu and J. Li, *Sci. China Chem.*, 2011, **54**, 167-172.
- 75 X. Li, Y. Cheng, S. Kang and J. Mu, *Appl. Surf. Sci.*, 2010, **256**, 6705-6709.
- 76 G. C. C. Yang and S. W. Chan, *J. Nanopart. Res.*, 2009, **11**, 221-230.
- 77 J. Li, Z. Guo, Y. Wang and Z. Zhu, *Micro. Nano. Lett.*, 2014, **9**, 65-68.
- 78 Y. Wu, F. Xu, D. Guo, Z. Gao, D. Wu and K. Jiang, *Appl. Surf. Sci.*, 2013, **274**, 39-44.
- 79 W. Teng, X. Li, Q. Zhao and G. Chen, *J. Mater. Chem. A*, 2013, **1**, 9060-9068.
- 80 M. Lee and K. Yong, *Nanotechnology*, 2012, **23**, 194014.
- 81 Z. Wei, Y. Li, S. Luo, C. Liu, D. Meng, M. Ding and G. Zeng, *Sep. Purif. Technol.*, 2014, **122**, 60-66.

- 82 W. Zhou, Y. Guan, D. Wang, X. Zhang, D. Liu, H. Jiang, J. Wang, X. Liu, H. Liu and S. Chen, *Chem-Asian J.*, 2014, **9**, 1648-1654.
- 83 Y. Ni, W. Wang, W. Huang, C. Lu and Z. Xu, *J. colloid. Interf. Sci.*, 2014, **428**, 162-169.
- 84 R. T. Thomas, P. Abdul Rasheed and N. Sandhyarani, *J. colloid. Interf. Sci.*, 2014, **428**, 214-221.
- 85 Q. J. Xiang, J. G. Yu and M. Jaroniec, *Chem. Soc. Rev.*, 2012, **41**, 782-796.
- 86 H. Fu, T. Xu, S. Zhu and Y. Zhu, *Environ. Sci. Technol.*, 2008, **42**, 8064-8069.
- 87 Y. Long, Y. Lu, Y. Huang, Y. Peng, Y. Lu, S. Z. Kang and J. Mu, *J. Phys. Chem. C*, 2009, **113**, 13899-13905.
- 88 D. Chen, K. Wang, D. Xiang, R. Zong, W. Yao and Y. Zhu, *Appl. Catal. B: Environ.*, 2014, **147**, 554-561.
- 89 F. Wang, S. Min, Y. Han and L. Feng, *Superlattice. Microst.*, 2010, **48**, 170-180.
- 90 X. Li, D. Wang, G. Cheng, Q. Luo, J. An and Y. Wang, *Appl. Catal. B: Environ.*, 2008, **81**, 267-273.
- 91 F. Deng, L. Min, X. Luo, S. Wu and S. Luo, *Nanoscale*, 2013, **5**, 8703-8710.
- 92 Y. Min, K. Zhang, W. Zhao, F. Zheng, Y. Chen and Y. Zhang, *Chem. Eng. J.*, 2012, **193-194**, 203-210.
- 93 S. Gayathri, P. Jayabal, M. Kottaisamy and V. Ramakrishnan, *J. Appl. Phys.*, 2014, **115**.
- 94 S. Dong, Y. Li, J. Sun, C. Yu, Y. Li and J. Sun, *Mater. Chem. Phys.*, 2014, **145**, 357-365.

- 95 T. Hasobe, S. Hattori, P. V. Kamat and S. Fukuzumi, *Tetrahedron*, 2006, **62**, 1937-1946.
- 96 J. X. Sun, Y. P. Yuan, L. G. Qiu, X. Jiang, A. J. Xie, Y. H. Shen and J. F. Zhu, *Dalton. Trans.*, 2012, **41**, 6756.
- 97 M. Fu, J. Liao, F. Dong, H. Li and H. Liu, *J. Nanomater.*, 2014, **2014**, 1-8.
- 98 Q. Luo, L. Bao, D. Wang, X. Li and J. An, *J. Phys. Chem. C*, 2012, **116**, 25806-25815.
- 99 F. F. Li, D. F. Yang, M. S. Xia, Y. Wang and Y. S. Jiang, *J. Inorg. Mater.*, 2011, **26**, 917-922.
- 100 J. Y. Zheng, S. H. Bao, Y. Guo and P. Jin, *ACS Appl. Mater. Inter.*, 2014, **6**, 5940-5946.
- 101 G. Chen, M. Sun, Q. Wei, Y. Zhang, B. Zhu and B. Du, *J. Hazard. Mater.*, 2013, **244**, 86-93.
- 102 Y. C. Nah, I. Paramasivam and P. Schmuki, *Chemphyschem*, 2010, **11**, 2698-2713.
- 103 X. Chen, L. Liu, P. Y. Yu and S. S. Mao, *Science*, 2011, **331**, 746-750.
- 104 J. Su, Y. Zhang, S. Xu, S. Wang, H. Ding, S. Pan, G. Wang, G. Li and H. Zhao, *Nanoscale*, 2014, **6**, 5181-5192.
- 105 F. Duan, Q. Zhang, Q. Wei, D. Shi and M. Chen, *Prog. Chem.*, 2014, **26**, 30-40.
- 106 P. Madhusudan, J. Yu, W. Wang, B. Cheng and G. Liu, *Dalton. Trans.*, 2012, **41**, 14345-14353.
- 107 S. Dong, J. Feng, Y. Li, L. Hu, M. Liu, Y. Wang, Y. Pi, J. Sun and J. Sun, *Appl. Catal. B: Environ.*, 2014, **152**, 413-424.

- 108 S. Dong, C. Yu, Y. Li, Y. Li, J. Sun and X. Geng, *J. Solid State Chem.*, 2014, **211**, 176-183.
- 109 C. Yu, S. Dong, J. Feng, J. Sun, L. Hu, Y. Li and J. Sun, *Enviro Environ. Sci. Pollut. R.*, 2014, **21**, 2837-2845.
- 110 L. Hu, S. Dong, Y. Li, Y. Pi, J. Wang, Y. Wang and J. Sun, *J. Taiwan Inst. Chem. E.*, 2014, **45**, 2462-2468.
- 111 X. J. Dai, Y. S. Luo, W. D. Zhang and S. Y. Fu, *Dalton. Trans.*, 2010, **39**, 3426-3432.
- 112 J. Shang, W. Hao, X. Lv, T. Wang, X. Wang, Y. Du, S. Dou, T. Xie, D. Wang and J. Wang, *Acs Catal.*, 2014, **4**, 954-961.
- 113 J. Ding, S. Sun, J. Bao, Z. Luo and C. Gao, *Catal. Lett.*, 2009, **130**, 147-153.
- 114 J. W. Tang, Z. G. Zou and J. H. Ye, *Res. Chem. Intermediat.*, 2005, **31**, 513-519.
- 115 Y. Li, S. Dong, Y. Wang, J. Sun, Y. Li, Y. Pi, L. Hu and J. Sun, *J. Mol. Catal. A-Chem.*, 2014, **387**, 138-146.
- 116 S. Dong, Y. Cui, Y. Wang, Y. Li, L. Hu, J. Sun and J. Sun, *Chem. Eng. J.*, 2014, **249**, 102-110.
- 117 D. Channei, B. Inceesungvorn, N. Wetchakun and S. Phanichphant, *J. Nanosci. Nanotechnol.*, 2014, **14**, 7756-7762.
- 118 L. Zhang, W. Wang, S. Sun, D. Jiang and E. Gao, *Crystengcomm*, 2013, **15**, 10043-10048.
- 119 X. Zhao, H. Liu, Y. Shen and J. Qu, *Appl. Catal. B: Environ.*, 2011, **106**, 63-68.
- 120 S. Kant, S. Kalia and A. Kumar, *J. Alloy. Compd.*, 2013, **578**, 249-256.

- 121 C. Singh, S. Bansal and S. Singhal, *Physica B-Condens. Mat.*, 2014, **444**, 70-76.
- 122 W. Shi, J. Shi, S. Yu and P. Liu, *Appl. Catal. B: Environ.*, 2013, **138**, 184-190.
- 123 W. Du, X. Wang, H. Li, D. Ma, S. Hou, J. Zhang, X. Qian and H. Pang, *J. Am. Ceram. Soc.*, 2013, **96**, 2979-2986.
- 124 J. M. Song, H. Q. Hu, X. Z. Wang, S. J. Zhao, Y. L. Shi and M. S. Ren, *J. Inorg. Mater.*, 2013, **28**, 1275-1280.
- 125 B. L. Fei, W. Li, J. H. Wang, Q. B. Liu, J. Y. Long, Y. G. Li, K. Z. Shao, Z. M. Su and W. Y. Sun, *Dalton. Trans.*, 2014, **43**, 10005-10012.
- 126 P. D. Kanhere, J. Zheng and Z. Chen, *J. Phys. Chem. C*, 2011, **115**, 11846-11853.
- 127 R. Xing, L. Wu, Z. Fei and P. Wu, *J. Environ. Sci-China*, 2013, **25**, 1687-1695.
- 128 V. Štengl, S. Bakardjieva, N. Murafa, V. Houšková and K. Lang, *Micropor. Mesopor. Mater.*, 2008, **110**, 370-378.
- 129 N. Soltani, E. Saion, W. M. M. Yunus, M. Erfani, M. Navasery, G. Bahmanrokh and K. Rezaee, *Appl. Surf. Sci.*, 2014, **290**, 440-447.
- 130 C. Tan, G. Zhu, M. Hojamberdiev, K. S. Lokesh, X. Luo, L. Jin, J. Zhou and P. Liu, *J. Hazard. Mater.*, 2014, **278**, 572-583.
- 131 X. Zheng, S. Meng, J. Chen, J. Wang, J. Xian, Y. Shao, X. Fu and D. Li, *J. Phys. Chem. C*, 2013, **117**, 21263-21273.
- 132 C. Yu, L. Wei, J. Chen, Y. Xie, W. Zhou and Q. Fan, *Ind. Eng. Chem. Res.*, 2014, **53**, 5759-5766.
- 133 I. S. Cho, D. W. Kim, S. Lee, C. H. Kwak, S. T. Bae, J. H. Noh, S. H. Yoon, H. S. Jung, D. W. Kim and K. S. Hong, *Adv. Funct. Mater.*, 2008, **18**, 2154-2162.

- 134 K. Ding, B. Chen, Z. Fang and Y. Zhang, *Theor. Chem. Acc.*, 2013, **132**, 1352.
- 135 X. Wang, G. Liu, Z.-G. Chen, F. Li, G. Q. Lu and H. M. Cheng, *Chem. Lett.*, 2009, **38**, 214-215.
- 136 H. Guo, Y. Ke, D. Wang, K. Lin, R. Shen, J. Chen and W. Weng, *J. Nanopart. Res.*, 2013, **15**, 1475.
- 137 S. Liang, R. Liang, L. Wen, R. Yuan, L. Wu and X. Fu, *Appl. Catal. B: Environ.*, 2012, **125**, 103-110.
- 138 W. J. Kim, D. Pradhan, B.-K. Min and Y. Sohn, *Appl. Catal. B: Environ.*, 2014, **147**, 711-725.
- 139 X. Zhang, J. Qin, Y. Xue, P. Yu, B. Zhang, L. Wang and R. Liu, *Sci. Rep-UK*, 2014, **4**, 4596.
- 140 X. Bai, L. Wang, R. Zong, Y. Lv, Y. Sun and Y. Zhu, *Langmuir*, 2013, **29**, 3097-3105.
- 141 Y. Li, W. Xie, X. Hu, G. Shen, X. Zhou, Y. Xiang, X. Zhao and P. Fang, *Langmuir*, 2010, **26**, 591-597.
- 142 L. Luo, A. T. Cooper and M. Fan, *J. Hazard. Mater.*, 2009, **161**, 175-182.
- 143 Y. He, L. Zhang, X. Wang, Y. Wu, H. Lin, L. Zhao, W. Weng, H. Wan and M. Fan, *RSC Adv.*, 2014, **4**, 13610-13619.
- 144 S. T. Gadge and B. M. Bhanage, *RSC Adv.* 2014, **4**, 10367-10389.
- 145 J. An and Q. Zhou, *J. Environ. Sci.*, 2012, **24**, 827-833.
- 146 C. Zhao, M. Pelaez, X. Duan, H. Deng, K. O'Shea, D. Fatta-Kassinos and D. D. Dionysiou, *Appl. Catal. B: Environ.*, 2013, **134-135**, 83-92.

- 147 G. Li, Y. Zhang, L. Wu, F. Wu, R. Wang, D. Zhang, J. Zhu and H. Li, *RSC Adv.*, 2012, **2**, 4822-4828.
- 148 S. Higashimoto, R. Shirai, Y. Osano, M. Azuma, H. Ohue, Y. Sakata and H. Kobayashi, *J. Catal.*, 2014, **311**, 137-143.
- 149 A. A. Ismail, L. Robben and D. W. Bahnemann, *Chemphyschem*, 2011, **12**, 982-991.
- 150 S. Higashimoto, Y. Hatada, R. Ishikawa, M. Azuma, Y. Sakata and H. Kobayashi, *Curr. Org. Chem.*, 2013, **17**, 2374-2381.
- 151 H. B. Y. Smida, M. Beicheickh and B. Jamoussi, *J. Residuals Sci. Tech.*, 2013, **10**, 47-54.
- 152 R. M. Mohamed and E. Aazam, *Desalin. Water Treat.*, 2013, **51**, 6082-6090.
- 153 L. Wang, X. Li, W. Teng, Q. Zhao, Y. Shi, R. Yue and Y. Chen, *J. Hazard. Mater.*, 2013, **244-245**, 681-688.
- 154 J. Yang, J. Dai and J. Li, *Environ. Sci. Pollut. R.*, 2012, **20**, 2435-2447.
- 155 H. Chen, X. Zheng, Y. Chen and H. Mu, *RSC Adv.*, 2013, **3**, 9835-9842.
- 156 K. S. Yao, D. Y. Wang, C. Y. Chang, K. W. Weng, L. Y. Yang, S. J. Lee, T. C. Cheng and C. C. Hwang, *Surf. Coat. Tech.*, 2007, **202**, 1329-1332.
- 157 J. Zhang, Y. Liu, Q. Li, X. Zhang and J. K. Shang, *Acs Appl. Mater. Inter.*, 2013, **5**, 10953-10959.
- 158 S. Dong, L. Hu, J. Feng, Y. Pi, Q. Li, Y. Li, M. Liu, J. Sun and J. Sun, *RSC Adv.*, 2014, **4**, 64994-65003.

Biography and photograph of several authors:

1. Dr Jianhui Sun

Dr Jianhui Sun (Professor, Henan Normal University, China) obtained his PhD in Environmental Sciences at the Guangzhou Institute of Geochemistry, Chinese Academy of Sciences, China. His water environment and pollution control research laboratory at the School of Environment, Henan Normal University is active in the field of photocatalysis, advanced oxidation technology, wastewater treatments and developing new approaches/concepts suitable for water and energy related applications. He has published over 50 research papers in the peer reviewed journals of international repute (h-index = 18). Dr Sun has teaching experience in courses of Environmental Monitoring and Environmental Pollution Control.



2. Dr Jingyu Sun

Dr Jingyu Sun received a BSc in Materials Sciences and Engineering from Zhejiang University, China in 2008, where he obtained an honored degree from the Mixed Class, Chu Kochen Honors College. He obtained his DPhil in 2013 from the Department of Materials, University of Oxford, UK for his work regarding the controlled growth of carbon nanomaterials on perovskite substrates. He is currently a postdoctoral associate in the Center for Nanochemistry, Peking University, where he works on graphene synthesis and related applications.



3. Dr Shuying Dong

Dr Shuying Dong received her PhD degree in Environmental Sciences in 2014 at the School of Environment, Henan Normal University, China under the supervision of Dr Jianhui Sun. She has engaged in the research in the field of photocatalysis for water treatment for more than 7 years and published 13 research papers in



the peer reviewed journals in such area. She is currently an assistant professor at the School of Environment, Henan Normal University. Her current research interests centers on the rational synthesis and mechanism exploration of visible-light-responsive photocatalysts for wastewater treatment.

4. Dr Maohong Fan

Dr Maohong Fan is an SER Professor in Chemical and Petroleum Engineering at the University of Wyoming, USA. He has led and worked on many projects in the areas of chemical production, clean energy generation and environmental protection, which have been supported by various domestic and international funding agencies such as



NSF, DOE and EPA in the USA, and industrial companies such as Siemens and Caterpillar. He has published over 175 refereed books, book chapters, and papers in different chemical and environmental engineering, energy, and chemistry journals.

Figure captions:

Figure 1. SEM images of the as-synthesized ZnO nanoclusters (a) and ZnO/RGO nanocomposites (b). (c) The degradation efficiencies of the metronidazole-contained wastewater by using the ZnO nanoclusters and ZnO/RGO nanocomposites under visible light irradiation. (d) Cycling runs of the ZnO/RGO nanocomposites for the photo-degradation of metronidazole. Reproduced with permission from ref. 94.

Figure 2. Representative TEM micrographs of different shaped BiVO₄ hierarchical structures obtained by varying the pH values of the precursors using NH₃·H₂O (a) pH = 4.9; (b) pH = 6.26; (c) pH = 6.72; (d) pH = 7; (e) pH = 7.38 and NaOH (f) pH = 4.9; (g) pH = 6.26; (h) pH = 7 as the pH controlling agent. Photocatalytic degradation of RhB under natural sunlight irradiation over (i) A-BiVO₄ and (j) S-BiVO₄ samples prepared at different pH values of the precursors. Reproduced with permission from ref. 107.

Figure 3. The HRTEM images of the prepared ZnSnO₃ hollow nanosphere (a) and ZnSnO₃/RGO nanocomposites (b). (c) The UV-Vis absorption spectra of the RGO, pure ZnSnO₃ hollow nanosphere and ZnSnO₃/RGO nanocomposites. The speculated illustration (d) and degradation efficiencies (e) of the metronidazole wastewater by ZnSnO₃ hollow nanosphere and ZnSnO₃/RGO nanocomposites photocatalysts under visible light irradiation. Reproduced with permission from ref. 33.

Figure 4. Visible-light-driven photocatalytic activity of g-C₃N₄/SmVO₄ composites with different g-C₃N₄ concentration (a) and 70 wt.% g-C₃N₄/SmVO₄ calcined at different temperatures (b). (c) Cycling runs for the photocatalytic degradation of RhB in the presence of 70 wt.% CS-450 sample under visible light irradiation. (d) A schematic for electron-hole separation and transport at the visible-light-driven g-C₃N₄/SmVO₄ composite photocatalyst interface. (e) Photoluminescence spectra of pure g-C₃N₄ and g-C₃N₄/SmVO₄ composite. (f) Transient photocurrent response for SmVO₄, g-C₃N₄ and 70 wt.% CS-450 samples. Reproduced with permission from ref. 35.

Figure 5. Influence of TBA (10 mM), NaN₃ (5 mM), KI (10 mM) and catalase (6 unit/L) on photocatalytic degradation of OTC by NF-TiO₂ under visible light at pH 5.5 (a) and 8.5 (b) (OTC 5 mg/L). (c) The initial rate of OTC photolytic degradation per unit of concentration at various initial concentrations at pH 5.5 and 8.5 under visible and solar light. (d) The proposed pathway of OTC photolytic degradation. Reproduced with permission from ref. 146.

Figure 6. (a) SEM image of SnIn₄S₈ nanostructure. (b) Schematic diagram for the photocatalytic reduction of Cr(VI) ions by SnIn₄S₈ under visible light irradiation. (c) UV-vis diffuse reflectance spectra of the samples SIS, SIS-PVP and SIS-CTAB. Inset: plots of $(Ah\nu)^2$ versus $h\nu$ for calculating the band gap energy. (d) A comparison on the photocatalytic reduction of aqueous Cr(VI) over the as prepared samples and the commercial P25 TiO₂ under visible light irradiation. (e) UV-vis absorbance spectrum

of the $K_2Cr_2O_7$ solution in the presence of the SIS-PVP products under visible-light irradiation. The inset shows the photographs of the solution before and after reaction. (f) Photocatalytic reduction of aqueous Cr(VI) over the sample SIS-PVP with five times of cycling use. Reproduced with permission from ref. 153.

Figure 7. The photocatalytic disinfection mechanism of TiON/PdO photocatalyst on the *Fusarium graminearum* macroconidia under visible light irradiation. Reproduced with permission from ref. 157, copyright (2013) American Chemical Society.

Table 1. Comparison of optical properties, band-gap values and BET surface areas of several reported photocatalysts.

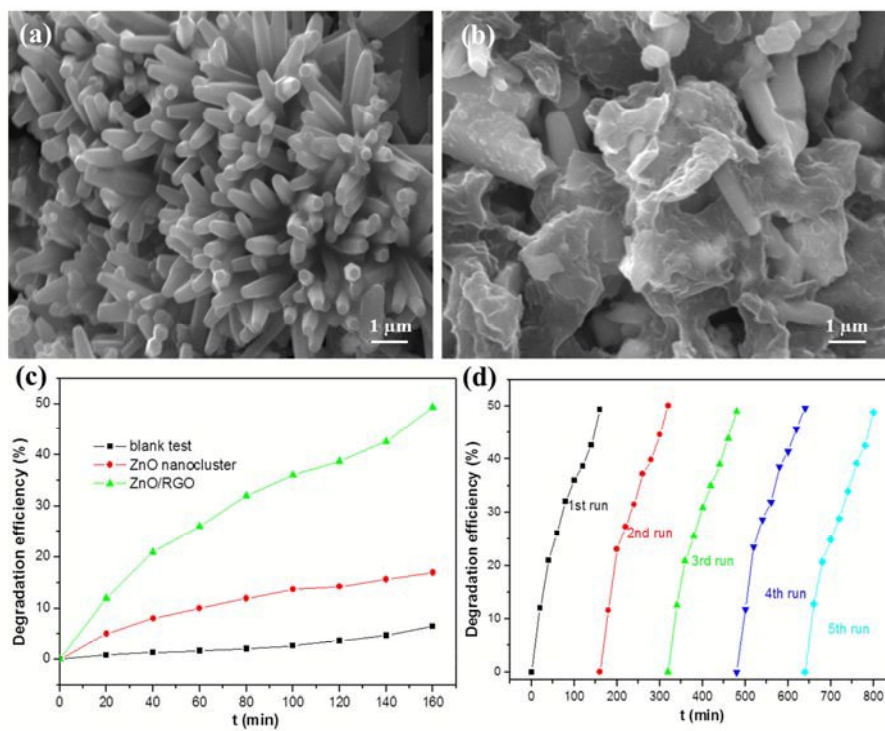


Figure 1

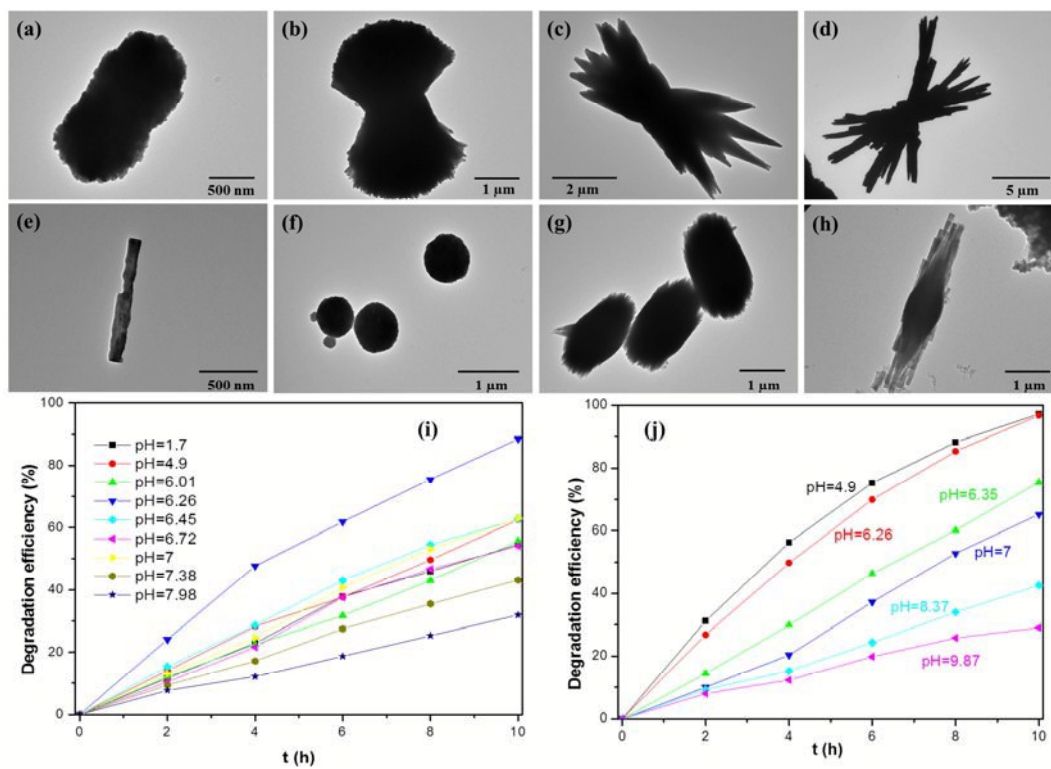


Figure 2

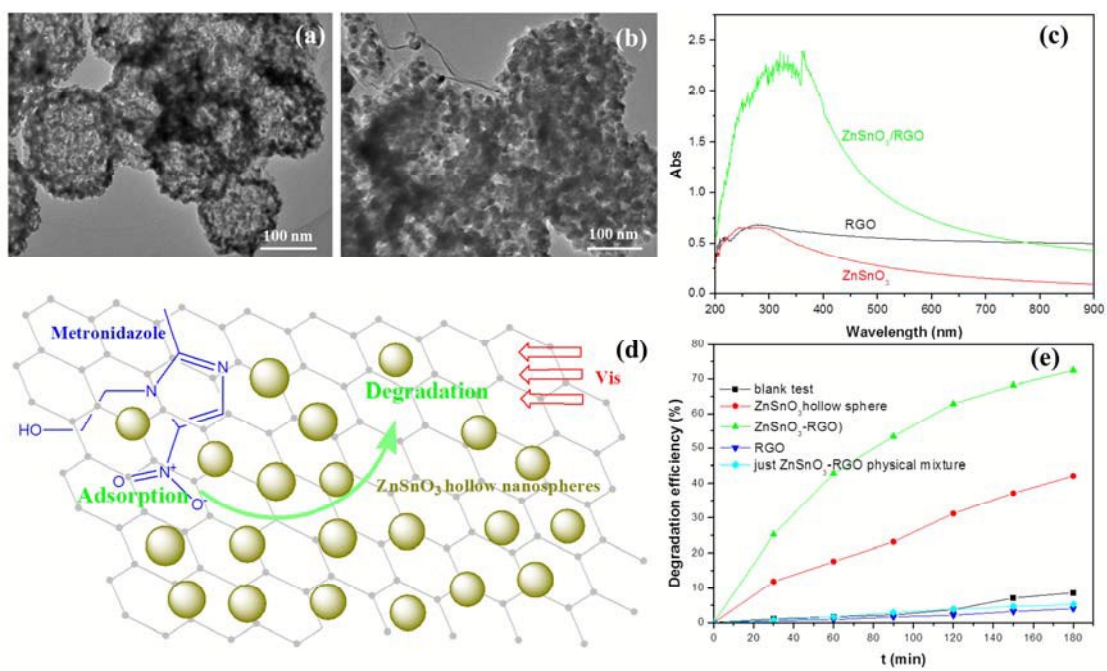


Figure 3

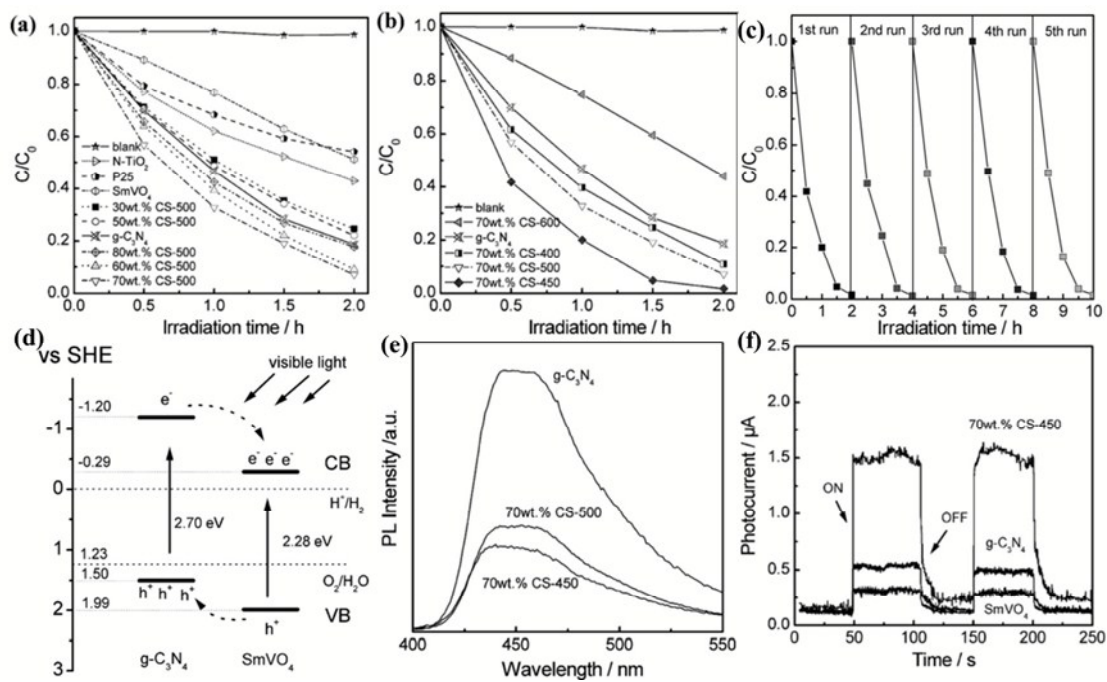


Figure 4

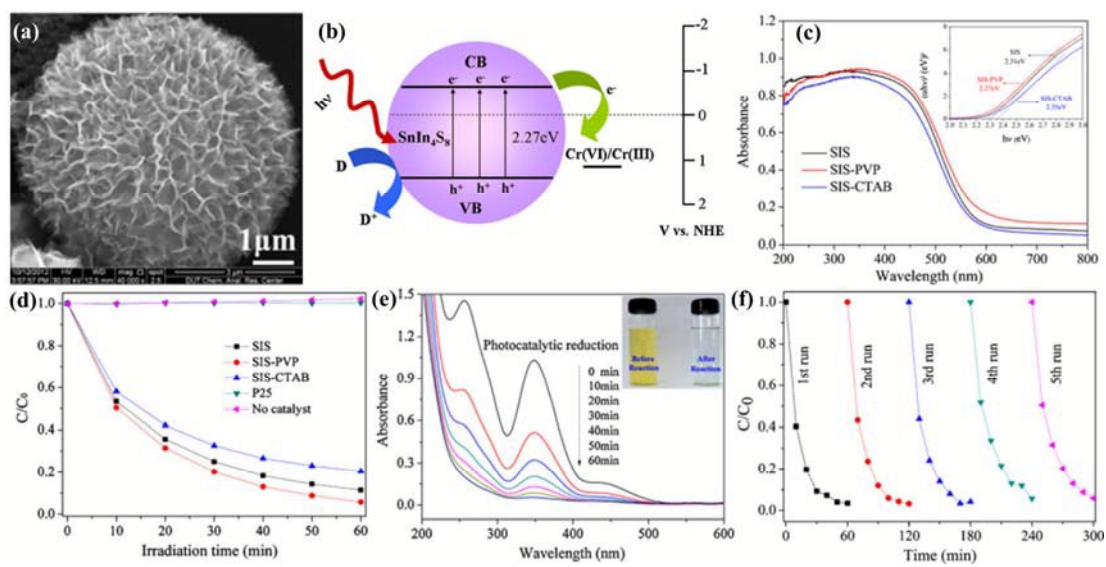


Figure 6

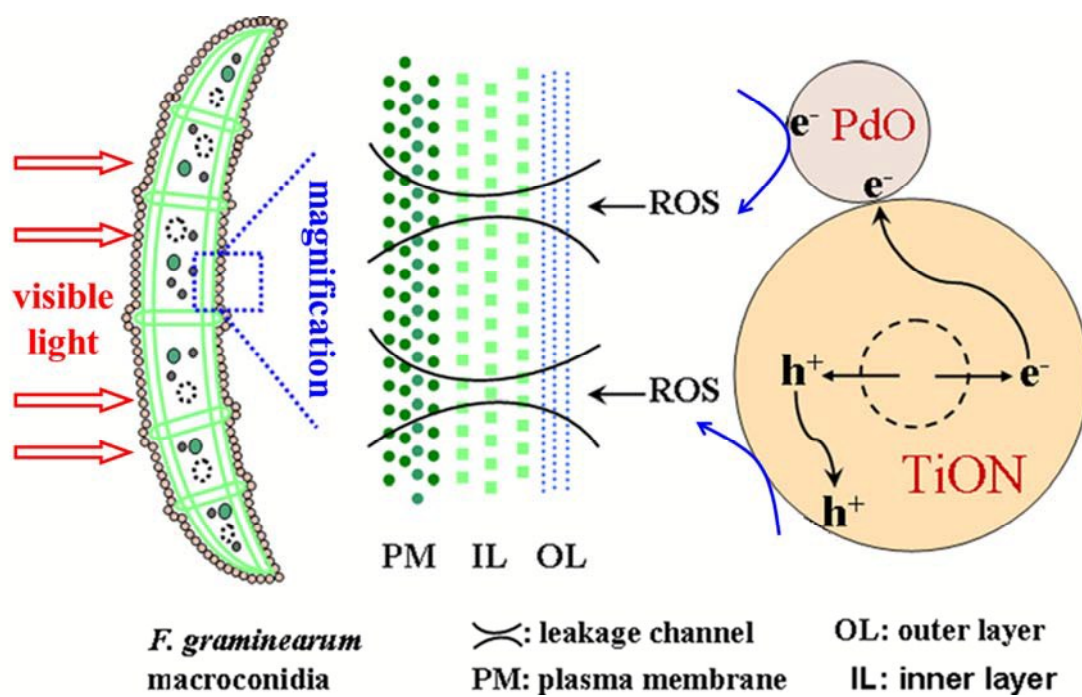


Figure 7

Table 1

Photocatalyst	Synthesis method	Optical properties and band gap	BET surface area ($\text{m}^2 \cdot \text{g}^{-1}$)	Pollutant	Degradation efficiency or reaction rate	Crystalline phase	Ref
WO ₃ -TiO ₂ /AC	Sol-gel	-	323	10 mg·L ⁻¹ Congo Red	62.52%	Anatase	53
			357		65.76%		
			386		64.91%		
			413		73.28%		
			456		75.34%		
			439		71.16%		
			514		79.35%		
			542		82.21%		
C-doped Bi ₂ O ₃	Calcination	Visible-light absorption band around 450-530 nm, the absorption edge of the C-doped Bi ₂ O ₃ has an obvious red-shift compared with the pure Bi ₂ O ₃	5.9	13 mg·L ⁻¹ methyl orange	95%	Monoclinic	61
			1.7		42%		
Bi ₂ O ₃							

TiO ₂	Hydrothermal	TiO ₂ nanotubes absorbed moderately	261.7	Acetaldehyde	0.0005 min ⁻¹	Anatase	66
0.1 mol % Pt-TiO ₂		around 385 nm and strongly	226.7		0.0028 min ⁻¹		
0.5 mol % Pt-TiO ₂		around 300-350 nm, the optical absorption of Pt-TiO ₂ was enhanced significantly in the region of 300-700 nm. The band gap of the TiO ₂ and Pt-TiO ₂ were calculated to be TiO ₂ (3.16 eV), 0.1 mol % Pt-TiO ₂ (3.11 eV), 0.5 mol % Pt-TiO ₂ (3.05 eV), 1 mol % Pt-TiO ₂ (3.01 eV), 2 mol % Pt-TiO ₂ (2.96 eV), 4 mol % Pt-TiO ₂ (2.64 eV)	203.9		0.0034 min ⁻¹		
1 mol % Pt-TiO ₂			163.6		0.0012 min ⁻¹		
2 mol % Pt-TiO ₂			141.8		0.0009 min ⁻¹		
4 mol % Pt-TiO ₂			139.9		0.0005 min ⁻¹		
C-N-TiO ₂ (N(0))	Microwave assisted solvothermal reaction	Compared with those of commercial P25 powders, the absorption edges of the prepared samples apparently shifted to the visible range. The bandgap	59.0	5 mg·L ⁻¹ RhB	48%, 0.0049 min ⁻¹	Anatase	69
C-N-TiO ₂ (DEA)					69.7		

C-N-TiO ₂ (TMA)		energies deduced from the tangent line are 3.16, 3.11, 2.98, 2.85, and 2.77 eV for P25, N(0), DEA, TMA, and DETA, respectively	63.7		min ⁻¹ 92%, 0.0397 min ⁻¹		
C-N-TiO ₂ (DETA)			129.1		10%, 0.0017 min ⁻¹		
TiO ₂		TiO ₂ showed an absorption threshold at 406 nm and a band gap energy of	46.6		35.6%		
N-TiO ₂	Acid catalysed sol-gel	3.05 eV; N-TiO ₂ showed a slight red-shift, giving a band gap of 3.02 eV;	78.5	20 mg·L ⁻¹ phenol	41.9%	Anatase	70
N-Pt-TiO ₂		N-Pt-TiO ₂ had the longest absorption edge and the highest absorbance in visible light region, giving a band gap of 2.58 eV	94.5		100%		

ZnO	Hybridized interaction	Both ZnO and C ₆₀ -ZnO showed the absorbance edge from 400 to 800 nm, the absorption intensity changed with the increasing of the C ₆₀ amount	57.3	3 mg·L ⁻¹ MB	85%, 0.0337 min ⁻¹	Hexagonal	86
C ₆₀ -ZnO			56.9		95%, 0.0569 min ⁻¹		
4.9 wt% g-C ₃ N ₄ -ZnO	Calcination	The absorption edges of g-C ₃ N ₄ -ZnO composite samples shift significantly to longer wavelengths as compared to ZnO, as well as band gap narrowing.	36	3 mg·L ⁻¹ Methyl Orange or p-nitrophenol	15.6 wt% g-C ₃ N ₄ -ZnO exhibited the best photocatalytic performance	Both ZnO and g-C ₃ N ₄ phases,	96
8.4 wt% g-C ₃ N ₄ -ZnO			75				
15.6 wt% g-C ₃ N ₄ -ZnO			33				
58.1 wt% g-C ₃ N ₄ -ZnO			28				
A-BiVO ₄ (pH=4.9)	Hydrothermal	The absorption edges for both the A-BiVO ₄ and S-BiVO ₄ samples blue shift eventually as the pH	10.3	5 mg·L ⁻¹ RhB	61 %	Monoclinic scheelite	107

A-BiVO ₄ (pH=6.26)		values of the precursors increase. As for A-BiVO ₄ , the absorption edge is measured to be at approx. 560 nm (pH 4.9), 555 nm (pH 6.26), and 540 nm (pH 7); as 590 nm (pH 4.9), 540 nm (pH 6.26), and 525 nm (pH 7) for S-BiVO ₄ .	4.6		89 %		
A-BiVO ₄ (pH=7)		The estimated band-gap energies of A-BiVO ₄ were to be approx. 2.40 eV (pH 4.9), 2.43 eV (pH 6.26), and 2.45 eV (pH 7), respectively, whereas for S-BiVO ₄ ,	1.6		62 %		
S-BiVO ₄ (pH=4.9)		the band-gap energies were measured to be approx. 2.28 eV (pH 4.9), 2.40 eV (pH 6.26), and 2.45 eV (pH 7).	6.3		97 %		
S-BiVO ₄ (pH=6.26)			4.6		96 %		
S-BiVO ₄ (pH=7)			11.1		61 %		